AHMED ZABANA University of RELIZANE.
FACULTY OF SCIENCE AND TECHNOLOGY.

Revue
Des Matériaux
&
Energies Renouvelable

Vol 5, N°2, 2021.

Published on: November, 1st 2021.

ISSN: 2507-7554

E- ISSN: 2661-7595

Rechearch Review of Scences and Technologies

Editorial

Our journal is a leading international journal on topics concerning materials and renewable energy and their developments in the industrial world. Published since 2016, the journal focused on two axes of materials and their evolution according to their potential applications and renewable energy.

Revue des Matériaux et énergies renouvelables is a top-rated international journal on topics concerning materials and renewable energy and their developments in the industrial world. Published since 2016, the journal has always focused on the materials and renewable energy and their evolution regarding to their potential applications.

In this sense, this issue presents original work in this field either from chemistry for the definition or design of new materials to structural mechanics to assess the lifespan of structures made from these materials or to give ideas for the development of renewable energy.

The editorial board

Summary

N°	Title	Authors	Page from - to
01	Estimation and Technico-Economic Analysis of the Wind Power Potential in North of Cameroon	Dawoua Kaoutoing Maxime, Sadam Alphonse, Kitmo, Miguiri Blaise.	1 - 6
02	Etude de la caractérisation d'un éco-matériau« Béton auto-plaçant (BAP) à base de fibres végétales »	MAROUF Hafida, ABDOULAYE Amine Sadadine, MORKACHE Mohammed Abdelhakim.	7 -16
03	Rheological behaviour of Fresh Cement Pastes Formulated from a Self Compacting Concrete	Farih Messaoudi, Hafida Marouf, Messaoud Moudjari.	17 - 23
04	NUMERICAL MODELING OF THE EVOLUTION OF THE STRAIN ENERGY ALLSE OF THE CRACK PROPAGATION BY THE X-FEM METHOD	Bentahar Mohammed, Benzaama Habib, Mahmoudi Noureddine.	24 - 31
05	Numerical Simulation of Forced Convection in Receiver of two Concentrators: dish parabolic and trough parabolic	Djermane Kenza, Kadri Syham.	32 - 39

Revue des Matériaux et Energies Renouvelable Vol 5, N°2, 2021
ISSN : 2507-7554
***E*- ISSN** : 2661-7595

Revue des Matériaux & Energies Renouvelable

Journalhome : https://www.univ-relizane.dz
ISSN : 2507-7554
***E*- ISSN** : 2661-7595

Estimation and Technico-Economic Analysis of the Wind Power Potential in North of Cameroon

Open Access

Dawoua Kaoutoing Maxime[a*],Sadam Alphonse[b*], Kitmo[c], Miguiri Blaise[b]

[a*]Faculty of Mines, and Petroleum Industries, University of Maroua, P.O Box: 46Maroua, Cameroon
[b*]UFD PAI, Laboratory of analysis of simulation and testing, IUT de Ngaoundéré, P.O.Box 455, Ngaoundere, Cameroon
[c]Department of Renewable Energy, National Advanced School of Engineering of University of Maroua, Cameroon

Article history:

Received 02 June 2021.

Received in revised form 03 June 2021.

Accepted 07 August 2021.

Keys word: Evaluation, Technico-economic, Potential, cost, Wind Energy, Air Density

RESUME

An evaluation and a technico-economic study was conducted in this paper in the three cities of Cameroon on the wind potential. The model chosen is the model that takes into account the variation of the air density that varies with altitude. The technico-economic analysis is based on the wind energy. The results show that the cost per kWh varies with the city. By installing 6 Nordex wind turbines, this will help to solve the energy deficit problem in the North of Cameroon which has a good wind speed.

1. Introduction

The need for electrical energy in Cameroon is covered by hydroelectric dams. The various dams in operation in Cameroon are: the Song Lou Lou dam located on the Sanaga River with a capacity of 384 MW, the Nachtigal dam with a capacity of 3 TWh and the hydroelectric dam of Edéa. Given the growing demand for electrical energy, these do not fully cover the needs of the population. In recent years, the demand for power generation in Cameroon has increased rapidly due to population growth and industrialization. Many researchers are studying how to use energy sources such as solar, biomass and wind power as substitutes for traditional energy resources. At the same time, most countries are trying to use renewable energy to replace fossil fuels in order to preserve a better environment. Regarding wind energy, higher conversion rate, cleanliness and safety are its main advantages compared to other types of renewable energy compared to other types of renewable energy [1]. In the last two decades, global wind energy has been rapidly intensifying among the available renewable energy resources [2]. The lack of organized data on the country's wind potential, covering entire regions, has been one of the reasons for the limited applications in Cameroon. Within the framework of this work, it is a question of estimating the energy potential in each region of Cameroon and carrying out a technical-economic study.

2. Methodology

The average meteorological data (wind speed) were collected via the meteorological stations of Ngaoundéré, Garoua and Maroua. The processing of these data is done with the Matlab software.

2.1. Wind data processing

The choice of the analysis of the statistical wind data was made using the weibull distribution method. The wind distribution is done using the Weibull distribution given by equation 1[1].

$$f(V) = \left(\frac{K}{C}\right)\left(\frac{V}{C}\right)^{K-1}\exp\left(-\left(\frac{V}{C}\right)^{K}\right) \quad (1)$$

f(V) is the probability density of the velocity; K is the form factor of the Weibull distribution (dimensionless) and C is the scale factor of the Weibull distribution in m/s. K and C are determined by the EPF method. This method is more accurate and efficient [2]. K is determined using equation (2).

$$\mathrm{K} = 1 + \frac{3.69}{(\mathrm{Epf})^2} \quad (2)$$

Epf denotes the factor energy obtained as a function of the instantaneous velocity by the relation given by equation (3). Equation (4) gives the value of C.

$$\mathrm{Epf} = \frac{\frac{1}{\mathrm{n}}\sum_{\mathrm{i}=1}^{\mathrm{n}} \mathrm{Vi}^3}{\left(\frac{1}{\mathrm{n}}\sum_{\mathrm{i}=1}^{\mathrm{n}} \mathrm{Vi}\right)^3} \quad (3)$$

$$\mathrm{C} = \frac{VmK^{2.6674}}{0.184+0.8116K^{2.73855}} \quad (4)$$

2.2.Wind Speed Extrapolation

Wind turbines are generally located at distances greater than 10 m from the ground. At these heights, the wind has a good speed that can be used by the turbines. The wind speed used to calculate the recoverable power is then exploited at the height of the wind turbine mast. Equation (5) is used for this purpose [4].

$$V(z_2) = V(z_1)\left(\frac{\mathrm{Z}_2}{\mathrm{Z}_1}\right)^{\alpha} \quad (5)$$

$$\text{with}\ \alpha = \frac{1}{\ln\left(\frac{\bar{\mathrm{z}}}{\mathrm{zo}}\right)} - \left(\frac{0.0881}{1-0.00881\times\ln\left(\frac{\mathrm{z}_1}{\mathrm{z}_0}\right)}\right) \times \ln\left(\frac{V(\mathrm{z}_1)}{6}\right) \quad (6)$$

$$\text{and}\ \bar{\mathrm{z}} = \sqrt{\mathrm{z}_1 \times \mathrm{z}_2} \quad (7)$$

V(z) is the reference velocity measured at z meters from the ground; z velocity measurement altitudes z_1 and z_2 are the reference height and the variable value above the reference, respectively; z_0 is the ground roughness.

Extrapolation of Weibull parameters as a function of height

The following equations 8 and 9 are used to extrapolate the K and C values to a height z[4].

$$Kz = \frac{K_{10}}{1-0.00881\ln\left(\frac{\mathrm{z}}{10}\right)} \quad (8)$$

$$\mathrm{C_z} = \mathrm{C_{10}} \times \left(\frac{\mathrm{z}}{\mathrm{z_{10}}}\right)^{\mathrm{n}} \quad (9)$$

$$\text{with}\ \mathrm{n} = (0.37 - O.088\ln(\mathrm{C_{10}})) \quad (10)$$

2.3. Recoverable wind potential of the site

The wind turbine does not fully recover the wind speed and taking into account the altitude the recoverable power is the wind turbine does not fully recover the wind speed and taking into account the altitude the recoverable power is[5]:

$$\langle Pr \rangle = 0{,}295.(\rho_0 - 1{,}194.10^{-4}.h_m).\langle V^3 \rangle \text{en kW/m}^2 \quad (11)$$

$$\rho_{0=} 1{,}196 kg/m^3 \quad (12)$$

h_m is the elevation of the site from the sea.

The average maximum energy recoverable in one year is :

$$\langle Er \rangle = 0{,}295.24.365{,}25(\rho_0 - 1{,}194.10^{-4}.h_m).\langle V^3 \rangle \text{en kWh/m}^2 (13)$$

2.4. Output power of wind turbine

Taking note that of the fact that each wind turbine have its pover curve by the manufacturer, the output power of the wind turbine is:

$$\langle Pr \rangle = \frac{1}{2}.C_p(v).A.(\rho_0 - 1{,}194.10^{-4}.h_m).\langle V^3 \rangle \quad (14)$$

Where $C_p(v)$ is the power coefficient at a speed , A is a surface area of the wind turbine blades.

2.5. Estimation of the cost of energy

The factors governing the cost of energy are[2] (Gokcek, 2009):

-Investment cost (including auxiliary fees for findings, connection to the network, etc.),

-Operating and maintenance cost,

-Electricity production/average wind speed,

-The life span of the turbine,

-Discount rate,

-The total energy produced.

The factors governingthe present cost value (PVC) are:

- The lifetime of the machine (n) was assumed to be 20 years.

- The interest rate (r) and inflation rate (i) were taken to be 15 and 12%, respectively.

- Operation maintenance and repair cost (Comr) was considered to be 25% of the annualcost of the machine (machine price/lifetime).

-Scrap value S was taken to be 10% of the machine price and civil work.

-Investment (I) includes the machine price plus its 20% for the civil work and other connections.

The present cost value (PVC) of wind turbine (WT) is given in the following relationship[6];[7]; [8]:

$$PVC_{WT} = I_{WT} + c_{omr,WT}\left(\frac{1+i}{r-i}\right)\left[(1 - (\frac{1+i}{1+r})^n\right] - S_{WT}\left((\frac{1+i}{1+r})^n\right) \quad (15)$$

CostPer Unit (CPU) is [9]:

$$CPU = \frac{PVC_{WT}}{E_{served}} \quad (16)$$

Many parameters come into play for the choice of the wind turbine that corresponds to the chosen site. These parameters are: the starting speed, the nominal speed, the stopping speed, its length, the number of blades. The choice was oriented on Nordex wind turbines because of their starting speeds which correspond to the lowest speeds in each region.

3. **Results and discussion:**

Using meteorological stations, wind speeds at 10m from the ground in the three main cities in the far north of Cameroon (Ngaoundéré, Garoua, Maroua) were determined.

Table 1. Wind speed at 10m from the ground in Northern Cameroon

Month	Jan	feb	march	April	May	Jun	Jully	August	Sept	Oct	Nov	Dec	Town
Wind speed (m/s)	3.4	3.4	3.7	3.9	3.6	3.1	2.9	2.8	2.6	2.8	3.2	3.5	Ngaoundere
	3.8	3.8	4.1	4.3	3.9	3.3	3.1	2.9	2.7	3	3.5	4	Garoua
	4.1	4	4.4	4.6	4.2	3.5	3.2	3.1	2.8	3.2	3.8	4.3	Maroua

At 10m from the ground, the wind is disturbed by the forest and the houses. At higher heights, the wind has a good speed. For this reason, the wind speeds were extrapolated to different heights for each city. Figure 1 shows the wind speed at different heights in the city of Ngaoundéré. At 70m, this speed is 5.80 m/s in April. This is the maximum speed, which means that it is the most windy month in the city. The least windy month in this city is September with a wind speed of 3.87 m/s. Similarly, in the cities of Garoua and Maroua, at the same height, the most windy month is always April but with an increase in wind speed, in Garoua 6.4 m/s and 6.84 in Maroua. The least windy month is September. With a wind speed of 4.01 in Garoua and 4.16 in Maroua. Table 2 shows the estimated power produced in each region. The region with the highest wind power is the Far North with a power of 145,234 W/m2.

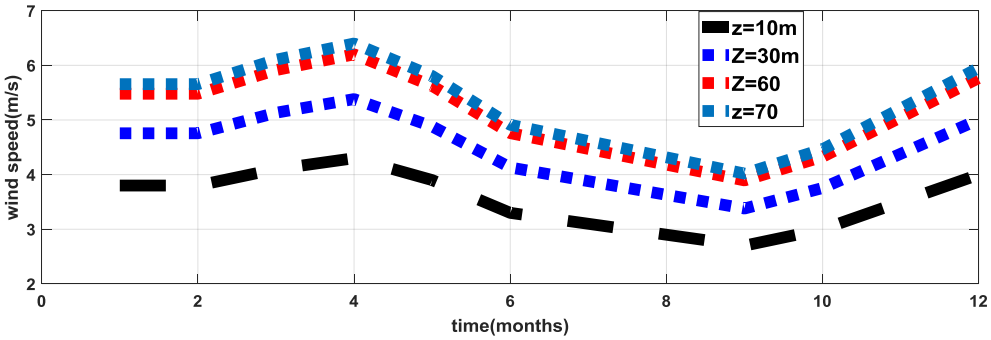

Figure 1. Extrapolated annual average speeds in Ngaoundere

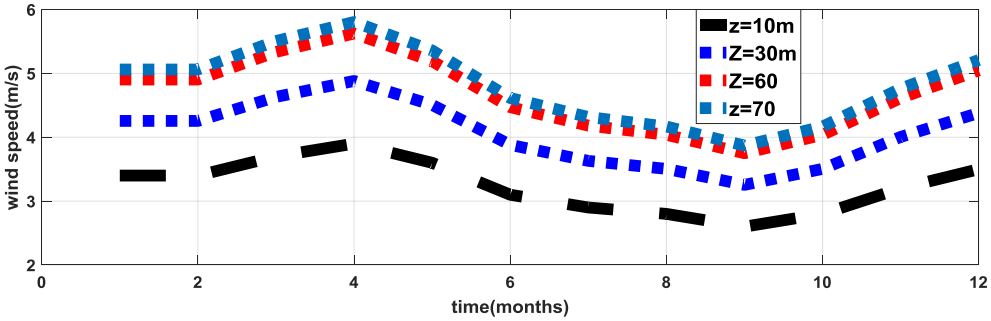

Figure 2. Extrapolated annual average speeds in Garoua

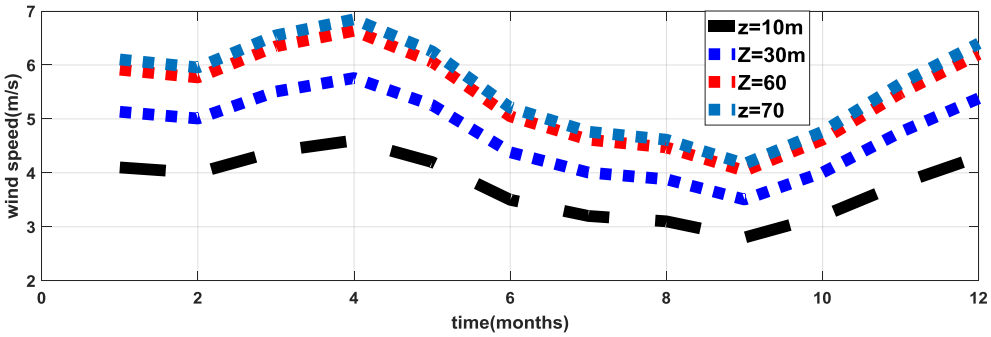

Figure 3. Extrapolated annual average speeds in Maroua

4. The choice of the wind turbine

Many parameters come into play for the choice of the wind turbine that corresponds to the chosen site. These parameters are: the starting speed, the nominal speed, the stopping speed, its length, the number of blades.

Table 2. Characteristics of Nordex wind turbines

Type of the wind turbine	**N29/250**	**N43/600**	**N54/1000**
Power rating (KW)	250	600	1000
Start-up speed (m/s)	3-4	3-4	3-4
Nominal speed (m/s)	15,5	13,5	14
Cut-off speed (m/s)	25	25	25
Diameter of rotor, m	27,5	43	54
Hub height, m	30, 40, 50	40, 50,60	50,60,70

The evaluation of the wind energy is done with the wind turbine type N43/600 because it has the lowest nominal speed (13.5 m/s) which corresponds to the wind speed in the North of Cameroon. Its nominal power is 600 kW.

Economic analysis

By installing a wind farm with 5 wind turbines to produce at least 31536 MWh annually and 11510.640 GWh over 20 years in the city of Maroua. 29541 MWh annually and 10782.465 GWh over 20 years in the city of Garoua. 21376MWh annually and 7802.240 GWh in Ngaoundéré. The economic analysis gives a cost of $0.347 in Ngaoundéré, $0.305 in Garoua and $0.297 in Maroua. This variation in the price per kilowatt-hour in these cities is influenced by differences in production

5. Conclusion

It was in this work to evaluate the energy potential in the three cities of Cameroon (Ngaoundere, Garoua and Maroua), the wind speeds were collected at 10 m from the ground. These speeds were extrapolated because the wind turbines are more than 10m above the ground. The Nordex type wind turbine (N43/600) for a height of 60 m was chosen. An economic study was made. It appears from this study that the cost of the kilowatt-hour is not the same in the three cities of Cameroon.

6. References

[1] S. Gaddada et S. P. K. Kodicherla, « Wind energy potential and cost estimation of wind energy conversion systems (WECSs) for electricity generation in the eight selected locations of Tigray region (Ethiopia) », *Renewables*, vol. 3, n° 1, p. 10, déc. 2016, doi: 10.1186/s40807-016-0030-8.

[2] M. Gökçek et M. S. Genç, « Evaluation of electricity generation and energy cost of wind energy conversion systems (WECSs) in Central Turkey », *Applied Energy*, vol. 86, n° 12, p. 2731‑2739, 2009.

[3] F. Boukli Hacene et L. Loukarfi, « Analyse statistique et élaboration d'un atlas éolien de la vallée du Cheliff », avr. 2021.

[4] J. L. Nsouandélé, D. K. Kidmo, S. M. Djetouda, et N. Djongyang, « Estimation statistique des données du vent à partir de la », *Revue des Energies Renouvelable*, vol. 19, n° N°2 (2016) 291-301, p. 12, 2016.

[5] S. Alphonse, J. Bikai, A. T. Fokone, et K. Cesar, « Potentiel énergétique éolien et profil de consommation d'énergie dans le village Wouro Kessoum Ngaoundéré Cameroun », *J. Ren. Energ.*, vol. 23, n° 1, Art. n° 1, nov. 2020.

[6] M. Sarkar et M. Hussain, « The potential of wind electricity generation in Bangladesh », *Renewable Energy*, vol. 1, n° 5, p. 855‑857, janv. 1991, doi: 10.1016/0960-1481(91)90038-Q.

[7] M. Li et X. Li, « MEP-type distribution function: A better alternative to Weibull function for wind speed distributions », *Renewable Energy*, vol. 30, p. 1221‑1240, juill. 2005, doi: 10.1016/j.renene.2004.10.003.

[8] A. W. Dahmouni, M. Ben Salah, F. Askri, C. Kerkeni, et S. Ben Nasrallah, « Assessment of wind energy potential and optimal electricity generation in Borj-Cedria, Tunisia », *Renewable and Sustainable Energy Reviews*, vol. 15, n° 1, p. 815‑820, janv. 2011, doi: 10.1016/j.rser.2010.07.020.

[9] J. F. Ngbara Touafio, O. Sanda, S. Malenguinza, J. M'Boliguipa, et R. M. Mouangue, « Analysis of a wind turbine project in the city of Bouar (Central African Republic) », *Scientific African*, vol. 8, p. e00354, juill. 2020, doi: 10.1016/j.sciaf.2020.e00354.

Revue des Matériaux et Energies Renouvelable Vol 5 N°2, 2021
ISSN : 2507-7554
***E*- ISSN** : 2661-7595

Revue des Matériaux & Energies Renouvelable
Journalhome : https://www.univ-relizane.dz
ISSN : 2507-7554
***E- ISSN** : 2661-7595*

FACULTE DES SCIENCES ET DE LA TECHNOLOGIE, UNIVERSITE DE RELIZANE.

Open Access

Etude de la caractérisation d'un éco-matériau « Béton auto-plaçant (BAP) à base de fibres végétales »

MAROUF Hafida [1], ABDOULAYE Amine Sadadine [2], MORKACHE Mohammed Abdelhakim [3]

[1] *Maitre de conferences B, Laboratoire LABMAT EnpOran-Maurice Audin, Département Genie Civil, Centre Universitaire Belhadj Bouchaib, Ain Témouchent, Algerie.*
[2] *Master II, Laboratoire de Pedagogie, Département Genie Civil, Centre Universitaire Belhadj Bouchaib, Ain Témouchent , Algerie.*
[3] *Master II, Laboratoire de Pedagogie, Département Genie Civil, Centre Universitaire Belhadj Bouchaib, Ain Témouchent , Algerie.*

Article history:

Received 24 July 2020.

Received in revised form 25 July 2020.

Accepted 13 December 2020.

RESUME

.Un béton auto-plaçant (BAP) est un béton fluide, très déformable et homogène qui se met en place par gravitation et sans l'utilisation d'un moyen de vibration. Il remplit parfaitement les formes des coffrages les plus complexes et voir même fortement ferraillés, il ne doit pas subir de ségrégation et doit présenter des qualités comparables à celles d'un béton vibré classique.
Ce travail a pour objectif de déterminer l'efficacité d'ajouter les fibres végétales au BAP.
A cet effet nous avons confectionné des bétons auto-plaçant avec fibres Alfa (2kg/m^3) et différents pourcentages de grignons d'olive 10%, 15% et 20% par substitution vis-à-vis les sables et les graviers 3/8 respectivement.
Les résistances mécaniques et aux attaques chimiques (durabilité) ont été déterminés et comparées à celle du béton témoin.
Les résultats expérimentaux montrent des comportements significatifs entre le BAP témoin et les BAP avec substitutions à l'état frais et à l'état durci.

Mots clés: *Béton auto-plaçant, , Fibre Alfa, Grignon d'olive, Durabilité, Végétaux*

BAP : Béton **A**uto-**P**laçant ; **S.C.C : S**elf-**C**ompacting **C**oncrete ; **BAP-T : B**éton **A**uto-**P**laçant **T**émoin ;
BAP-FA : Béton **A**uto-**P**laçant avec **F**ibre **A**lfa ; **BAP-G.O : B**éton **A**uto-**P**laçant avec **G**rignon d'**O**live ;
AFGC : Association **F**rançaise de **G**énie **C**ivil ;

* *Corresponding author. E-mail address: maroufhafida@yahoo.com*

1. INTRODUCTION

Dans une ère où le développement et l'expansion des industries prennent un niveau considérable au point de mettre en péril la stabilité environnementale de notre planète, une contrainte écologique se dévoile à l'horizon, signalant ainsi une alarme suite à la dévastation des ressources naturelles et faisant appel à la contribution scientifique dans le cadre de la valorisation de nouveaux procédés propice à cette terre qui nous abrite.

Le béton est un matériau qui a toujours accompagné le bâtiment moderne à travers ses majeures métamorphoses et d'innovations, a toujours mis en évidence le développement de ses propriétés qualitatives pour assurer son rôle primordial dans la portance des structures et le confort de ses utilisateurs. Tout type de fibres a été incorporé au béton afin de satisfaire plusieurs aspects rhéologiques et caractéristiques ; citons les fibres métalliques, synthétiques, végétales et mêmes hybrides en combinant deux types de fibres ou plus.

L'Algérie est un vaste territoire regroupant plusieurs zones climatiques et une énorme biodiversité florale où pousse la plante d'Alfa sur une superficie totale d'environ 4 000 000 ha, et dans le littorale où la filière oléicole occupe 389 000 ha. La production des déchets en Algérie a considérablement augmenté pendant ces dernières décennies. Cette augmentation est liée à la croissance démographique et au développement économique et social du pays. Tous ces produits et sous-produits issus de l'agriculture locale algérienne ne peut être mis à l'écart, une valorisation socio-économique de ces produits est à étudier.

C'est dans ce contexte que notre étude a pour objectif, en traitant le sujet d'élaboration de deux bétons auto-plaçant à base de fibres d'Alfa et de grignons d'olive, tout en le caractérisant et observant sa résistance aux agressions chimiques.

2. METHODE EXPERIMENTALE

Cette étude préliminaire sur la caractérisation à l'état durci des bétons auto-plaçant renforcés avec des ajouts végétaux (à savoir les fibres Alfa et les grignons d'olive), et afin d'être suffisamment pertinente dans notre analyse cinq compositions de BAP ont été testé dans le but d'évaluer l'apport des fibres Alfa et les Grignons d'olive sur le comportement des BAP. Les mélanges retenues et à étudiés :

- Béton autoplaçant « BAP» ;
- Béton autoplaçant non fibré (BAP témoin) « BAP-T »;
- Béton autoplaçant renforcé par des fibres Alfa « BAP-FA » ;
- Béton autoplaçant renforcé par des grignons d'olive « BAP-G.O » avec trois pourcentages différents 10 %, 15 % et 20 %.

2.1. MATERIAUX ET PROPORTIONS DES MELANGES

Avant d'entamer une formulation d'un béton, il est nécessaire de connaitre les matériaux utilisés à cet effet : Le ciment utilisé est un ciment Portland du Beni Saf CEM II/A-P 42.5N, Fillers calcaire issu de la carrière d'El Maleh, les Granulats qui sont des matériaux concassés de classes granulaires : du sable (0/4) et des gravillons de classes (4/8, 8/16), l'eau du robinet fournie par la société des eaux d'Oran SEOR au sein du Laboratoire de l'école national polytechniques d'Oran Maurice Audin, l'Adjuvant utilisé MEDAFLOW 30 avec une densité de 1,07 qui est un super-plastifiant/haut réducteur d'eau.

Les fibres alfa ajoutés au BAP sont d'une longueur de 2 cm et avec un diamètre proportionnel au diamètre des sables.

Les ajouts utilisés dans notre travail sont illustrés respectivement dans les figures suivantes :

FIGURE 1. ***Fibres Alfa***

FIGURE 2. ***Grignon d'olive***

2.2. OPTIMISATION DES MELANGES

Pour la formulation du béton auto-plaçant nous n'avons pas suivi une formulation classique. Nous avons respecté les conditions nécessaires permettant de garantir l'auto-plaçant tout en se basant sur des compositions proposées dans la littérature spécialisée **[1 – 2]**. Les fibres d'Alfa ont été substituées par rapport aux sables, soit environ 2 Kg/m^3 et les grignons d'olive ont été substitués à leur tour par rapport au gravier suivant les différents pourcentages.

TABLEAU 1. ***Proportion des bétons étudiés.***

Matériaux	Ciment	Filler	Sable	Gravier	Eau	Adjuvant
BAP – T	350	140	850	810	180	7.82
BAP – FA	350	140	848	810	180	7.82
BAP – G.O 10%	350	140	850	783	180	7.82
BAP – G.O 15%	350	140	850	769.5	180	7.82
BAP – G.O 20%	350	140	850	756	180	7.82

2.3. CARACTERISATION DES BETONS A L'ETAT FRAIS

Le comportement d'un BAP à l'état frais se différencie notablement de celui d'un béton ordinaire par : son ouvrabilité, sa mobilité en zone confinée et sa stabilité.

L'Association Française de Génie Civil [AFGC] [5] recommande trois essais principaux permettant la caractérisation du béton auto-plaçant à l'état frais mais on peut ajouter d'autres essais supplémentaires.

- Essai d'étalement au cône d'Abrams (Mobilité en milieu non confiné) ;
- Essai de la stabilité au tamis (Résistance à la ségrégation) ;
- Essai de la boîte en « L » (Mobilité en milieu confiné).

Le tableau ci-après présente les valeurs recommandées pour les différents essais de caractérisation du béton à l'état frais.

TABLEAU 2. ***Valeurs recommandées par les normes [3]***

Essais	**Essais Etalement (SF), mm**		**Stabilité au tamis (SR), %**		**Boite en L**		**T_{500}**	
					PL=(H_1/H_2)		**Secondes**	
Classes	SF1	550-650	SR1	≤20	PL1	≥0.8	VS1	<2
	SF2	650-750	SR2	≤15	PL2	≥0.8	VS2	≥2
	SF3	750-850		-		-		-

Voici les résultats obtenus des différents essais de caractérisation du béton à l'état frais

TABLEAU 3. ***Caractérisation du béton à l'état frais***

	BAP – T	BAP-F.A	BAP – G.O 10%	BAP – G.O 15%	BAP – G.O 20%
SF (mm)	830	625	635	725	700
PL=(H_2/H_1)	1	1	0,8	1	1
SR (%)	3,308	4,53	2,13	3,73	0,85
Masse volumique ρ (g/cm^3)	2,5	2,5	2,46	2,42	2,41

- ***Essai d'étalement :*** L'étalement des différents bétons est acceptable selon la norme NF EN 12350-8 et les recommandations de l'AFGC. On constate que l'étalement du béton témoin est beaucoup plus important que les autres types des bétons. Cette nuance est due à la présence des ajouts végétaux qui absorbent la totalité de l'eau de gâchage et cette insuffisance d'eau de gâchage engendre un béton un peu ferme ou qui présente une ouvrabilité moins importante. En raison de la présence de fibres d'Alfa dans le mélange du béton, on remarque une légère augmentation d'absorption en eau contrairement au mélange en grignons d'olive, cela est dû à la présence en surface d'une fine couche de matière grasse rendant les grignons d'olive plus étanche.
- ***Essai de la boite en L :*** On remarque aussi que toutes les variantes présentent un taux de remplissage supérieur ou égal à 0.8, donc les présentes compositions respectent le critère de l'écoulement en milieu confiné selon la norme NF EN 12350-1. Cela prouve que tous les différents types de bétons ont une grande fluidité à travers les barres d'acier, sauf le béton avec 10 % des grignons d'olive qui est à la limite de l'admissible.
- ***Essai de la stabilité au tamis :*** D'après les résultats obtenus durant cet essai, on remarque que toutes les compositions ont une stabilité suffisante $0 < P < 15$ %, ce qui donne un béton homogène et stable. L'excès des grignons d'olive provoque une diminution de la laitance du béton, ce qui admet un faible pourcentage. Mais avec les différents pourcentages de substitution en grignons d'olive, on constate que le béton avec 15 % de grignon d'olive a libéré assez de la laitance par rapport aux autres pourcentages. L'ajout de fibres d'Alfa au béton a aussi amélioré la qualité de ce dernier. On peut déduire que la stabilité vis-à-vis de la ségrégation diminue avec l'augmentation des fibres Alfa, en conséquent on doit optimiser la laitance de la gâchée avec l'adjuvant afin de répondre aux exigences des normes en vigueurs NF EN 12350-11.
- ***Essai de la masse volumique du béton humide :*** On constate que tous les différents bétons ont presque les mêmes masses volumiques humides. On remarque que la plus grande valeur est celle du béton témoin et le béton avec les fibres Alfa. La masse volumique diminue avec l'ajout de G.O, plus le pourcentage de G.O augmente, plus la masse volumique du béton diminue. Cette variation est due au faible poids spécifique des grignons d'olive par rapport au poids des gravillons 3/8.

2.4. CARACTERISATION DES BETONS A L'ETAT DURCI

Les résistances mécaniques en compression sont des caractéristiques essentielles des bétons, et des paramètres fondamentaux de notre étude, par conséquent leur évolution a été suivie pour tous les bétons étudiés. La mise en place des éprouvettes s'est effectuée dans différents moules destinés aux corps d'épreuve correspondants aux essais programmés :

- Eprouvette cylindrique d'élancement : 11×22 cm^3 ;
- Eprouvette prismatique d'élancement : $7 \times 7 \times 28$ cm^3.

Avant le remplissage des moules on applique un lubrifiant sur les parois. Les bétons auto-plaçant n'ont subi aucune vibration. Toutes les éprouvettes ont été démoulées 24 heures après leur remplissage. Elles ont ensuite été placées dans les conditions ambiantes du laboratoire jusqu'à 28 jours.

FIGURE 3. ***Remplissage et démoulage des éprouvettes***

2.4.1. RESISTANCE A LA COMPRESSION DES BAP

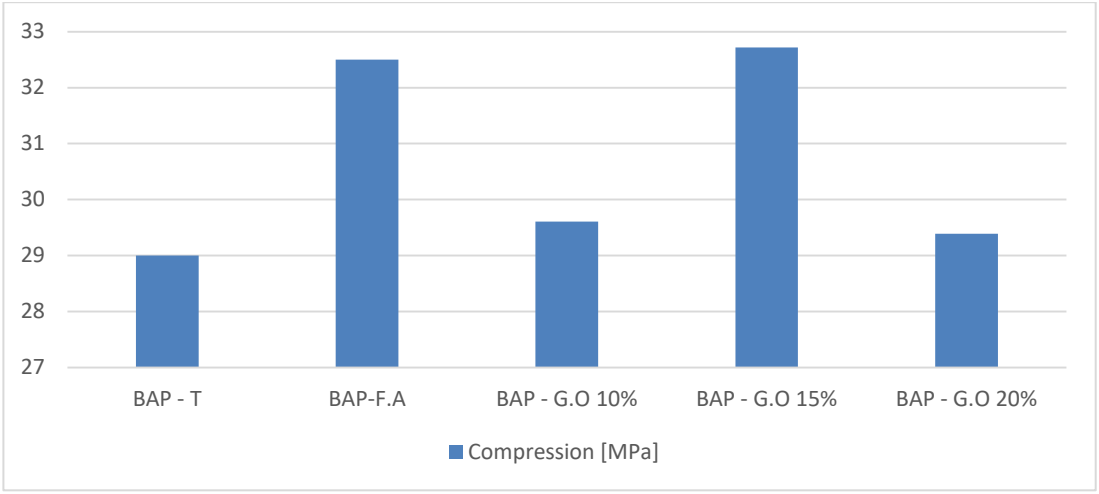

FIGURE 4. ***Résistance des différents bétons à la compression à 28 jours.***

Les grignons d'olive ont amélioré la résistance mécanique vis-à-vis le béton témoin et on constate aussi que la variante avec un pourcentage de 15 % a une résistance élevée par rapport aux autres variantes. Donc pour avoir une résistance appréciable du béton avec grignons d'olive, un certain pourcentage prescrit est à ne pas dépasser et ce dosage peut être optimal.

Tandis que les fibres Alfa ont développé une résistance assez supérieure à celle du béton témoin. L'ajout des fibres à une certaine limite a un apport positif sur la résistance mécanique en compression, car elles ont diminué la quantité d'eau (E/C) de gâchage par leurs comportements d'absorption et adsorption.

2.4.2. ESSAI A L'ULTRASON

TABLEAU 4. ***Essai Ultrasonique***

	BAP – G.O 10%	BAP – G.O 15%	BAP – G.O 20%
Vitesse de propagation (m/s)	6028	5805	5983

Selon les critères, toutes les différentes proportions des grignons d'olive dans le béton donnent une vitesse de propagation du son qui est supérieure à 4500 m/s. Donc notre béton a une appréciation excellente et n'amoindrie en aucun cas la qualité du béton.

3. LES ATTAQUES CHIMIQUES

La durabilité d'une structure donnée est définie comme étant la capacité de conservation de la structure dans des conditions telles que : garantir sa fiabilité et son esthétique, dans son environnement, avec le minimum possible coût de maintenance et les activités d'usage pour lesquelles elle a été conçue (fonctionnement structurel, sécurité et confort des usagers).

Donc les structures et les éléments en béton doivent avoir une bonne résistance face aux dégradations qui lui sont exposées, telles que les cycles de gel-dégel, les attaques chimiques, etc.

La porosité est l'élément indispensable qui définit la structure surfacique du béton, bien sûr qu'il existe plusieurs paramètres qui entrent en jeu mais c'est le paramètre qu'il faut fixer en premier lieu. Car il conditionne toutes les propriétés du béton. Le béton est connu par sa grande résistance en compression et celle-ci qui permet son utilisation dans la construction. Plus importante est sa résistance, plus faible est la porosité. Donc un béton plus résistant est aussi plus rigide mais est-il aussi durable ? [4]

3.1. ETUDE EXPERIMENTALE

Après 28 jours d'incorporation des différentes éprouvettes dans l'eau, on a procédé à l'essai de la durabilité sur une durée de deux mois. On a préparé trois différentes solutions : (Acide sulfurique : H_2SO_4, Acide chlorhydrique : HCl et l'Hydroxyde de Sodium : NaOH avec un pourcentage de 5%) afin d'exposer par immersion les différentes éprouvettes à ces solutions [4]- .

Le protocole expérimental des attaques des acides selon la norme : ASTM C267 – 96 est le suivant :

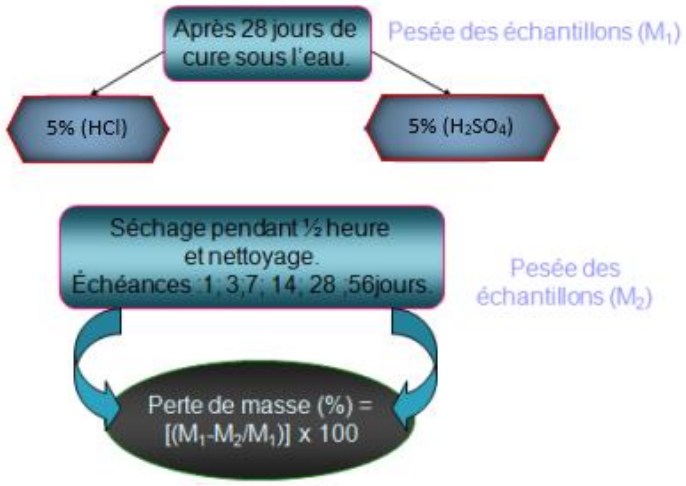

FIGURE 5. ***Le procédé suivi de la durabilité.***

FIGURE 6. ***Préparation des échantillons et des solutions chimiques.***

FIGURE 7. ***Immersion des éprouvettes dans les solutions chimiques.***

FIGURE 8. ***Détérioration des textures surfaciques.***

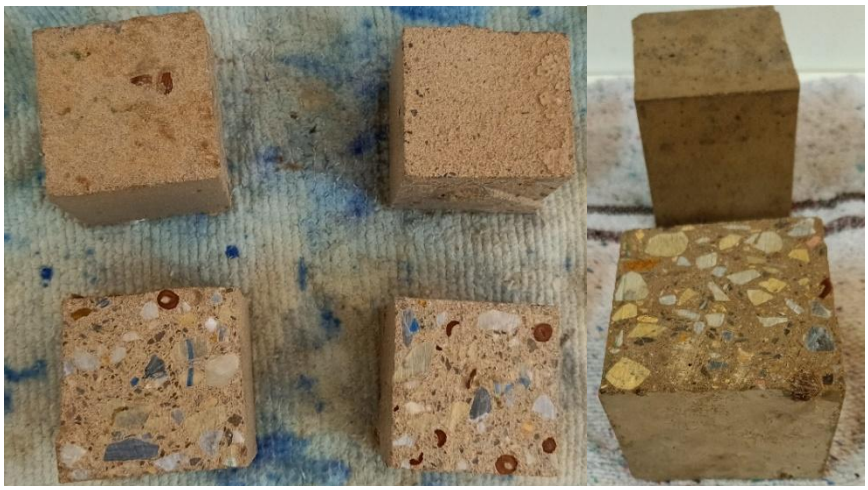

FIGURE 9. ***Contact visuel après la première semaine d'attaque des acides (H2SO4 et NaOH).***

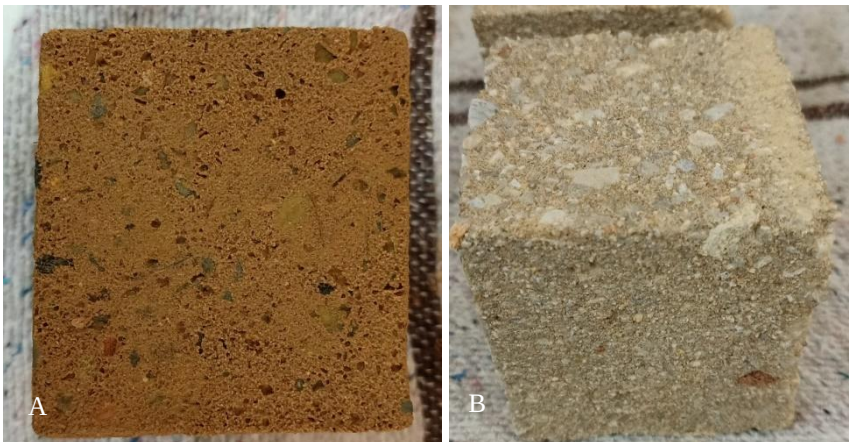

FIGURE 10. ***Contact visuel après la première semaine d'attaque des acides (HCl et H_2SO_4). A- détérioration du béton auto-plaçant avec fibre Alfa sous l'effet de HCl, B- détérioration du béton auto-plaçant sous l'effet de l'acide sulfurique.***

FIGURE 11. ***Détérioration des échantillons vis-à-vis de l'attaque de l'acide Sulfurique H2SO4 (A- béton auto-plaçant avec grignons d'olives, B-Béton auto-plaçant avec fibres Alfa).***

Les figures suivantes nous montrent la variation de la masse des échantillons en fonction du temps d'exposition pour différentes solutions.

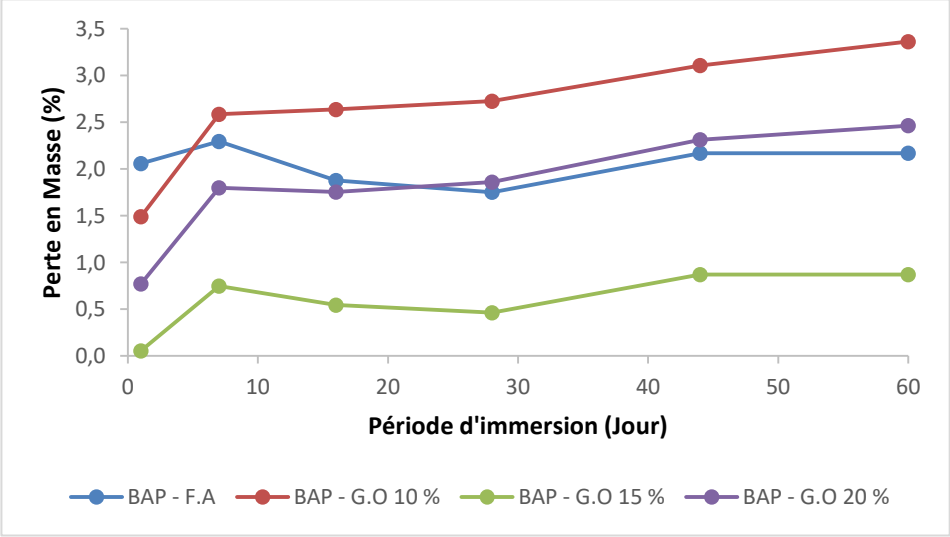

FIGURE 12. ***Perte de masse des différents échantillons sur une période d'immersion allant de 1 à 60 jours (5% HCl).***

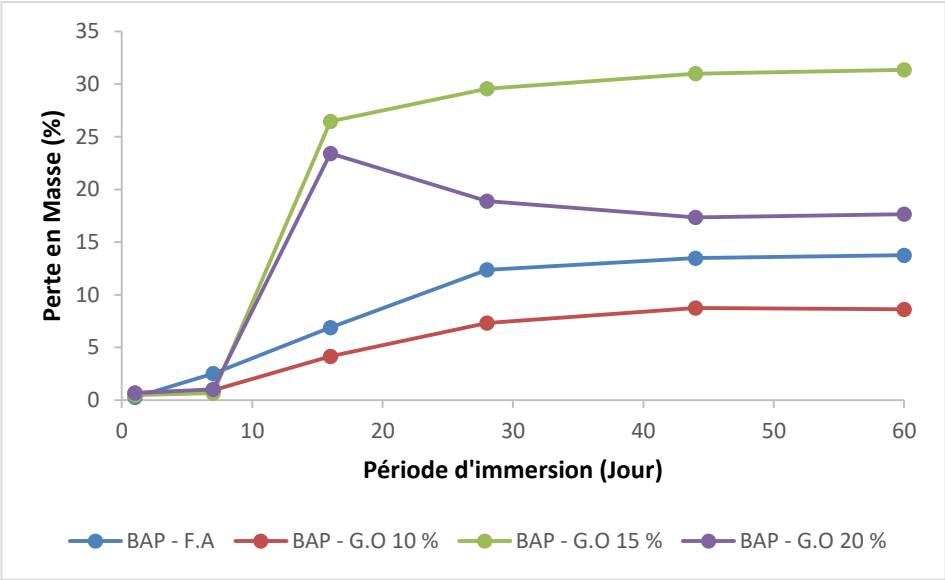

FIGURE 13. ***Perte de masse des différents échantillons sur une période d'immersion allant de 1 à 60 jours (5% H2SO4).***

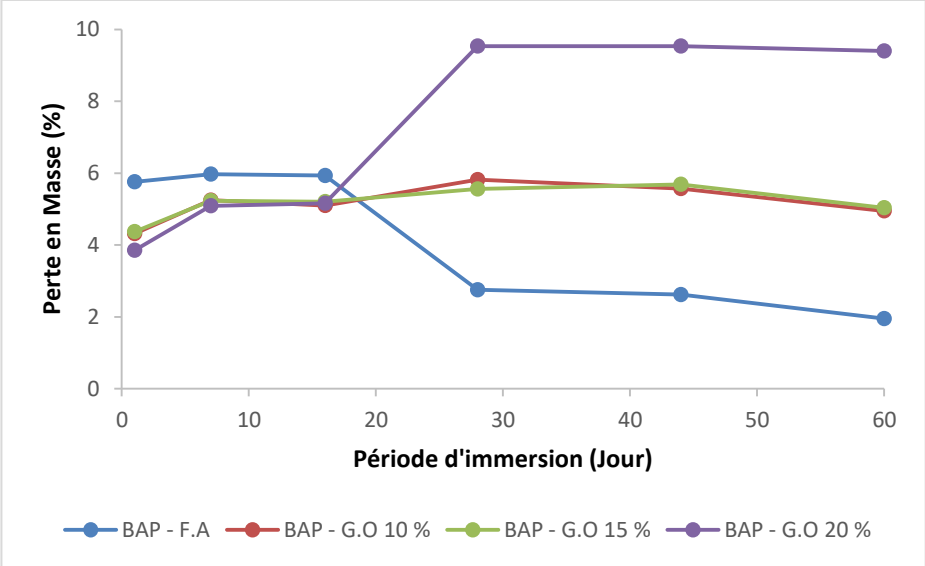

FIGURE 14. ***Perte de masse des différents échantillons sur une période d'immersion allant de 1 à 60 jours (5% NaOH).***

- Dans la FIGURE 12, on a constaté une perte massique permanente pour tous les différents échantillons immergés dans l'acide chlorhydrique (HCl) pendant les sept premiers jours.

Les bétons avec grignons d'olive (G.O) 10 % et 20 % ont presque le même type d'évolution de la variation massique durant l'attaque du HCl,

Entre les 7ème et 28ème jour, on a remarqué qu'il y a gain massique significative pour les bétons avec Alfa et G.O 15 %.

Au-delà du 16ème jour, il y a une perte massique progressive pour tous les échantillons.

Dès la première semaine, on a constaté une augmentation des pores au niveau de la texture (FIGURE 10) qui accélère la pénétration des agents agressifs.

- De la FIGURE 13, on remarque une chute massique brutale pendant les deux premières semaines et au-delà des deux premières semaines, la perte massique évolue d'une façon progressive pour les bétons avec Alfa et G.O 10 %.

Il y a une perte massique moins importante pendant la première semaine et brusquement une perte massique très importante durant la deuxième semaine pour les bétons avec G.O 15 % et 20 %. Au-delà de la deuxième semaine d'immersion, le béton avec G.O 15 % a maintenu sa perte massique progressive alors que le béton avec G.O 20 % a bénéficié d'un gain en termes de masse. Ce gain est dû au gonflement du béton induit par l'hydratation des grignons d'olive.

- On observe dans la FIGURE 14 que les bétons avec G.O 10 % et 15 % ont le même type de courbe et presque la même variation massique.

Une perte massique insignifiante a été remarquée pour tous les échantillons durant la première semaine et une conservation massique durant la deuxième semaine.

Au-delà de la deuxième semaine, un gain massique a été observé pour le béton avec Alfa tandis qu'une perte massique significative pour le béton avec G.O 20 %.

Les bétons avec G.O 10 % et 15 % n'ont pas subi une variation massique importante durant l'attaque chimique.

4. CONCLUSION

Notre travail a pour objet la mise en valeur des matériaux anodins au simple citoyen mais écologiques à notre environnement pour les spécialistes dans une ère où le bâtiment connait une extension importante et la commande accrue en matériaux de construction, et plus particulièrement en bétons ce qui met en cause l'exploitation massive des ressources naturelles pour compenser l'approvisionnement du marché des matériaux de construction.

Les fibres alfa ont joué un rôle remarquable dans l'ouvrabilité par leurs absorptions d'eau réduisant ainsi le rapport E/C initiale induisant par de suite à un excès de super-plastifiant pour rattraper le déficit met en cause la nécessité d'étudier la possibilité d'introduction d'un autre traitement de fibres que celui mis en œuvre dans notre compagne expérimentale.

Les grignons d'olive ont aussi contribué à la caractérisation de l'ouvrabilité du béton pour chaque pourcentage d'incorporation mais en générale le béton a marqué des résultats satisfaisants vis-à-vis la majorité des essais effectués.

L'étude de durabilité des bétons réalisés à l'encontre des attaques chimiques :

- ✓ Le mélange à base de fibres Alfa a montré une bonne résistance aux premiers temps mais s'affaiblit par l'effet des acides ;
- ✓ Pour le béton à base de grignons d'olive, chaque pourcentage présente un comportement hétérogène mais le plus remarquable est celui à dosage de 10% de grignons d'olive.

5. REFERENCES

[1]- KHAYAT K., « *Les bétons auto-nivelant : propriétés, caractérisation et applications* », Colloque sur les bétons auto-nivelant, Université de Sherbrooke, 1er novembre 1996.

[2]- *Le béton auto-plaçant édité par HOLCIM*, Suisse, version 2004, 32 pages.

[3]- LAIFA W., BEHIM M., TURATSINZA A., ALI-BOUCETTA T, « *Caractérisation d'un béton auto-plaçant avec addition de laitier cristallisé et renforcé par des fibres de polypropylène et de Diss* », Rev. Sci. Technol., Synthèse, 25: p 100-110, 2014.

[4]- KHELIFA, M. R. « Effet de l'attaque sulfatique externe sur la durabilité des bétons auto-plaçant », 2009 ;

[5]- [AFGC] Association Française de Génie Civil ;

Revue des Matériaux et Energies Renouvelable Vol 5 N°2, 2021
ISSN : 2507-7554
***E*- ISSN** : 2661-7595

Revue des Matériaux & Energies Renouvelable

Journalhome : https://www.univ-relizane.dz
ISSN : 2507-7554
E- ISSN : *2661-7595*

FACULTE DES SCIENCES ET DE LA TECHNOLOGIE, UNIVERSITE DE RELIZANE.

Rheological Behaviour of Fresh Cement Pastes Formulated from a Self Compacting Concrete

Open Access

***Farih Messaoudi*[1], *Hafida Marouf*[2*], *Messaoud Moudjari*[3]**

[1] *Department of Civil Engineering, Saad Dahlab University, Blida,09000, Algeria.*
[2*] *Department of Civil Engineering, Belhadj Bouchaib Center University, Ain Temouchent, 46000, Algeria.*
[3] *Department of Architecture and Town Planning, Algiers, 16000, Algeria.*

Article history:

Received 16 July 2020.

Received in revised form 17 July 2020.

Accepted 04 October 2020.

Keys word: Self-Placing Pastes; Marble Waste; Shear Threshold; Additives.

RESUME

The mineral additives and additives are introduced into the concrete to improve their rheological behavior in the fresh state, and their mechanical properties and durability in the cured state. In this study two sets of tests were conducted on self-placing pastes composed with marble waste as a mineral addition. The first series consists in determining the spreading of this pasta with the mini-cone; the second series consists in determining their shear threshold using the HAAKE RHEOSTRESS 1 rheometer.

A correlation between the results obtained on the results of spreading and those of the shear threshold, for the various compositions considering the influence of the super plasticizer and a viscosity agent is sought.

1. Introduction

The development of self-compacting concretes (BAP) and high-performance concretes is especially related to progress in the field of admixtures and the use of mineral additions [1-2]. Several models for predicting the rheological behavior of concretes is developed [3-5].

These models require control of the properties of concrete constituents, particularly the rheology of pasta [4-6]. Indeed, today's concretes are often composed of mineral additions, this presence has effects on the behavior of cementitious pastes and therefore the rheological behavior of concrete and all related properties, it is therefore necessary to study in their presence. In this study, we are interested in the rheological behavior of self-compacting (very fluid) pastes that are used in the composition of self-compacting concrete (BAP). The study is based on rheological test results using the HAAKE RHEOSTRESS 1 rheometer (Figure 1) and mini-cone spreading by varying the percentage of addition in the pasta, the amount of water, the super plasticizer dosage and the viscosity agent dosage. The ultimate goal of this study is to propose a rheological model that will correlate the results of spreading tests to the mini cone to those measured using the rheometer. The model will make it possible, from simple mini cone spreading tests, to predict the shear threshold of pasta.

* *Corresponding author. E-mail address: maroufhafida@yahoo.com*

2. MATERIALS AND EXPERIMENTAL PROCEDURES

2.1 Materials Used

The cement used is a CEM II / A 42.5 manufactured by the Lafarge cement factory located in Algeria conforming to the NF EN 197-1 standards. The super plasticizer used is a MEDAPLAST SP 40, the viscosity agent is CIMCIL L25; both adjuvants are produced by Granitex (Algeria).

The marble powder used is of economic interest because it is a recovery powder from waste marble. The waste is supplied in the form of a wet paste. The dough is dried; the clumps obtained are crushed and then sieved to recover fines with a diameter of less than 80 μm.

2.2 Experimental procedures

Two experimental programs are conducted. The first program to characterize the pasta rheology using the rheometer (Fig.1). The principle of the test is to shear a sample of dough between two trays with horizontal surfaces, one at rest and the other mobile (plane-plane geometry). This rheometer is equipped with a Rotor valve with an imposed speed. After adjustments, the gap between the two plates was validated to 1.5 mm. The tests are carried out at a temperature of 20 ° C (± 1 ° C). The protocol followed for our tests is: a pre-shear at 10 s-1 for 2 minutes before each ramp up speed. This step makes it possible to destructor the material and to obtain a state of reference identical to all the pastas. Then an increasing linear ramp of speed from 0 to 70 s-1 for 5 minutes is applied. The second program is carried out using the hollow frustoconical mini-cone for measuring pasta spreading (Fig. 1). Its dimensions in mm are: 40 of height, 70 of greater diameter and 80 of smaller diameter. The cone is placed in the center of a glass plate and filled with paste. It is then lifted to allow the dough to drain; two perpendicular measurements of spreading are performed.

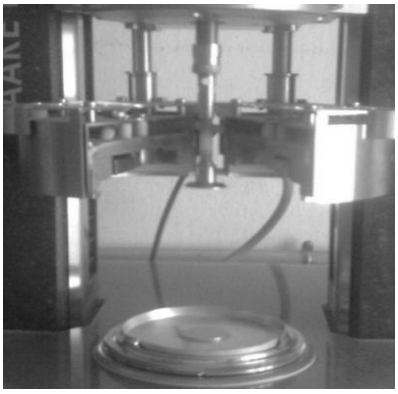

Figure 1– Haake Rheostress 1

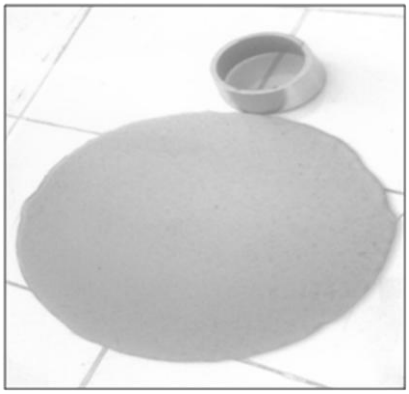

Figure 2– Spreading Test at the Mini-Cone.

2.3 Formulations studied

The compositions tested are summarized in the form of groups with each time one or two components that vary, they are formulated at constant masses is 500 g.

Abbreviations: SP: super plasticizer dosage; AV: viscosity agent dosage; W: water; C: cement; PM: marble powder. SP and AV are expressed as a percentage of the cement mass. The groups are summarized as follows:

• Groups (1, 2 and 3) formulated as follows: Group 1 [W/ (C + PM) = 0.40], Group 2 [W / (C + PM) = 0.45] and Group 3 [W / (C + PM) = 0.50]. For these 3 groups, 7 values of C / PM were tested and for each value of (C / PM fixed) one has a variable SP.

• Groups (4, 5 and 6) formulated as follows: Group 4 [W/ (C + PM) = 0.40], Group 5 [W / (C + PM) = 0.45] and Group 6 [W / (C + PM) = 0.50]. For these 3 groups we have (C / PM) = 2, the variable SP then the variable AV. For these cases, for a composition, the value of AV was first varied; then for each value of AV the SP was varied.

3. RESULTS AND DISCUSSIONS

3.1 Results at the Mini-Cone

The analysis of the results leads to understanding the combined effect of marble powder MP, SP and AV on the flow of self-placing pastes.

3.1.1. Results of Groups 1, 2 and 3 (without AV)

Figs. 3a, 3b and 3c correspond to the results of spreading as a function of the variation of the SP and of the C / PM ratio, ie the amount of PM in the pasta formulated at the same ratios.

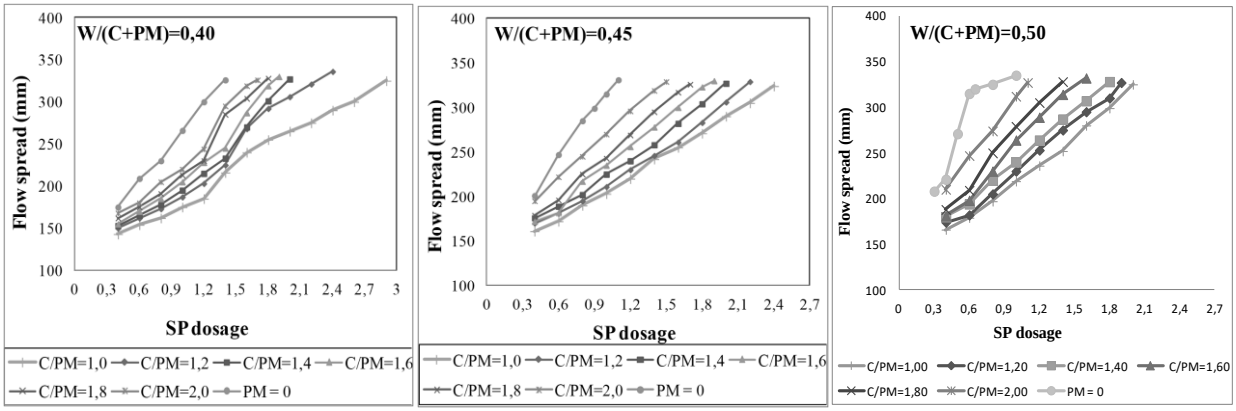

(3a) (3b) (3c)

Figure 3– Evolution of SP and C / PM spreading of Group 1, 2 and 3.

The figure 3 show that the spread for a given composition, the same ratios W / (C + PM) and C / PM, increases with the increase of the SP.

On the different mixtures, for the ratio W / (C + PM) fixed for example at 0.40 and for a fixed SP, the spread decreases with the increase of the quantity of the PM in the dough is therefore with the C / PM decreasing. In other words, for the same SP, the less marble powder is put into the composition, the more the dough is spread out well.

In fig. 4, we have shown the curves of variation of the spreading as a function of the C / PM ratio for an SP fixed at 1% that for the pasta formulated at different ratios W / (C + PM). Thus, for the example of the case where (W / (C + PM) = 0.40), the results show the increase of the spreading, 175 mm with a ratio of (C / PM = 1) and 220 mm for a report (C / PM = 2).

Now the SP is fixed, the substitution of the cement by the PM has an inversely proportional effect on the spreading of the paste. In this case, in order to thin the dough, the SP dosage must be increased.

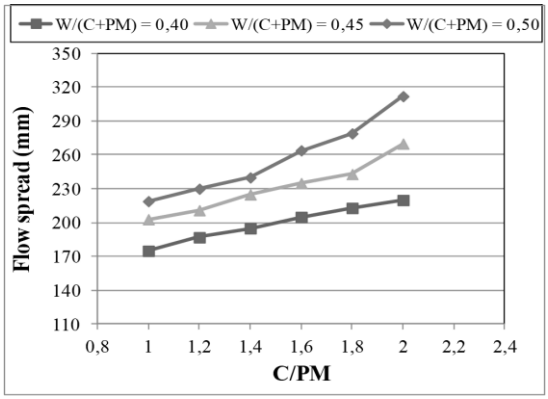

Figure 4– Evolution of the spread according to C / PM for a SP fixed at 1% and W / (C + PM) variable.

Certainly, the sprawl increases with the increase of the ratio (W / (C + PM)), ie with the quantity of water.

3.1.2. Results of Groups 4, 5 and 6 (with AV)

Because the results obtained on groups 4 and 6 are similar to those obtained on group 5, we have not shown in fig. 5, than those in group 5.

We then represented the spreads as a function of the variation of the SP in the abscissa and the AV from one curve to another, the C / PM ratio is fixed at 2, the pasta is formulated at a ratio: W / (C + PM) = 0.45.

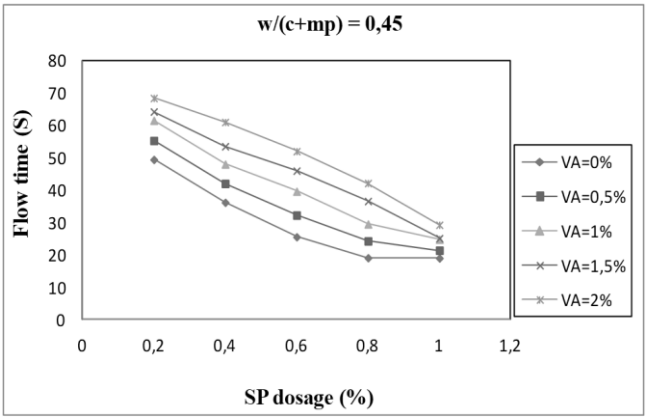

Figure 5– Evolution of the Spread According to the sp Dosage for Group 5

The results of figure 5 show that the introduction of the viscosity agent in the different compositions does not have a great influence on the spreading measurements.

The same behavior was observed on the other two groups formulated at a ratio W / (C + PM) = 0.40 and 0.50.

Indeed, on the three groups of pasta studied the difference in spreading between the pasta formulated at 0% of AV and the pasta formulated at 2% of AV, the spreading decreased on average by 18 mm, which is not important.

When the super plasticizer, its action is not influenced by the presence of the viscosity agent because the spread evolves in the same way, with the same differences, between the pasta with different viscosity agent dosages. This suggests that there was no chemical interaction between these two adjuvants.

3.2 Rheometer Results

In this part we studied the rheometer behavior of the different self-placing pastes tested without and with the viscosity agent. We studied the combined influence of PM content and SP on the shear threshold.

The rheograms recorded on the tested pasta follow a law of the Herschel-Bulkley type which is expressed by the relation (1). This result is consistent with what is found in the literature [6-7].

$$\tau = \tau_0 + b(\gamma)^c \qquad (1)$$

Where: $\tau 0$ is the shear threshold that corresponds to the ordinate at the origin of the rheogram, represents the shear rate, and b and c are constant in the model (rheological flow characteristics). As a reminder: when c = 1 and $\tau 0 \neq 0$, we find the Binghamian behavior; when c = 1 and $\tau 0 = 0$, we find the Newtonian behavior.

For (c> 1) the pasta has a rheo-thickening behavior and for (c <1) the pasta has a rheofluidifying behavior.

The curves obtained change parameters depending on the amount of powder added and the presence or absence of the superplasticizer or the viscosity agent.

3.2.1. Shear Threshold Results for Groups 1, 2 and 3 (without AV)

In fig. 6 the shear threshold versus SP curve is shown for groups 1 , 2 and 3 pasta.

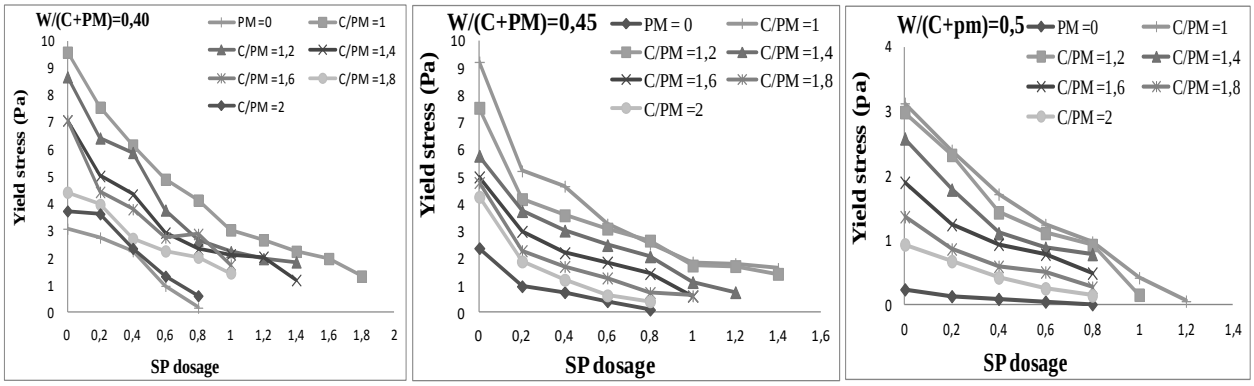

(6a) (6b) (6c)

Figure 6– Evolution of shear threshold versus SP of pasta groups 1, 2 and 3.

In these figures, it can be seen that for these pastes the measured shear threshold values decrease with the increase of the SP, while keeping the ratios W / (C + PM) and C / PM constant. When the substitution of the cement by PM, the more the PM increases (C / PM decreases), the higher the shear threshold, and therefore more super plasticizer is needed to fluidify the formulated pastes with the same ratio (W / (C + PM)). So the threshold increases with the substitution of the cement by the PM by keeping the SP constant.

On the other hand, it is also noted that the threshold values decrease with the increase of the ratio (W / (C + PM) that by comparing the three groups of graphs of figs 6. The observed decrease is slight between the same pulps with ratios (W / (C + PM) = 0.40 and 0.45) However, this drop is important between the ratio pulps (W / (C + PM) = 0.45 and 0.50).

3.2.3. Group 4, 5 and 6 Shear Threshold Results (with AV)

In figure 7 are shown the results of the shear threshold as a function of the variation of the AV and the SP, the ratio C / PM is fixed at 2.

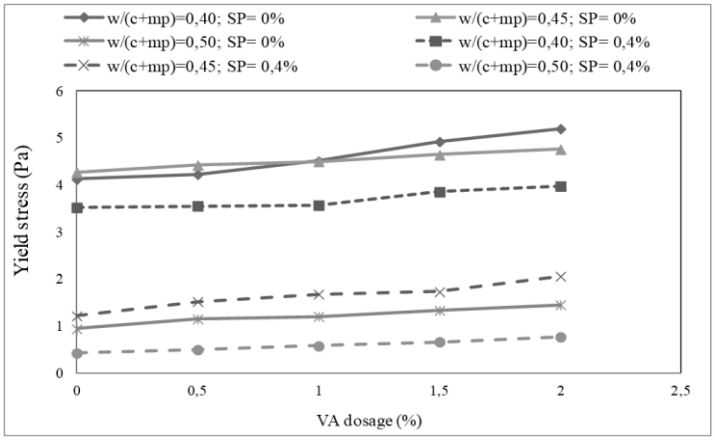

Figure 7– Evolution of the Shear Threshold as a Function of AV and SP of the Pasta of Groups 4, 5 and 6.

For figure 7 it is noted that for these pasta the values of the measured shear threshold evolve with a slight increase with the increase of the AV, while maintaining (W / (C + PM), C / PM and SP) constant. This result is consistent with the use of viscosity agents which are often used to make viscous materials without affecting their fluidity (shear threshold).

In addition, in the presence of the viscosity agent, it is found that the introduction of SP at a dosage of 0.4% has lowered the shear threshold. The drop produced between formulas without SP and those at 0.4% SP is uniform (remains almost constant with the variation of AV) because the curves evolve in parallel.

On the other hand, we note that the threshold values decrease with the increase of the ratio (W / (C + PM)).

4. CORRELATION BETWEEN SHEAR THRESHOLD AND SPREADING OF SELF-PLACING PASTES

The spread measurement results obtained at the mini-cone were used to establish a correlation with the shear threshold obtained by the rheometer.

4.1. Correlation between Spreading and Shear Threshold of Group 1, 2 and 3 Results (without AV)

In figure 8 we have shown the experimental results of spreading as a function of the measured shear threshold values for pastes formulated without AV.

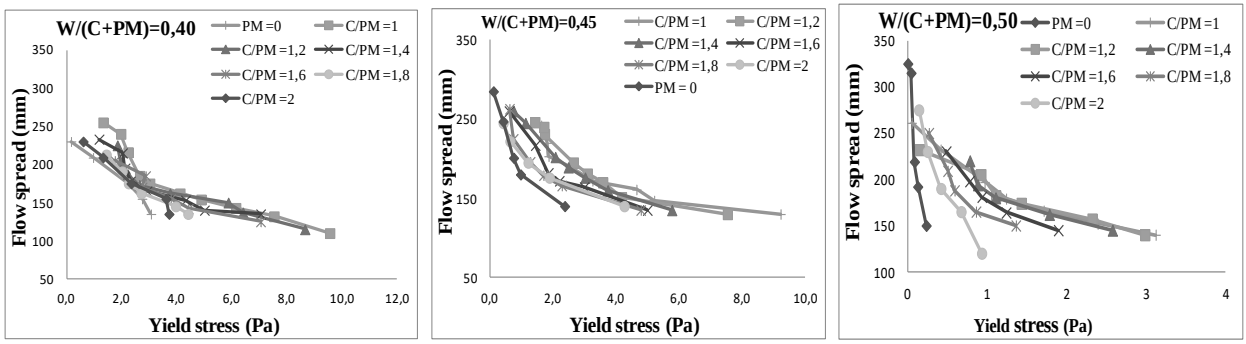

(8a) (8b) (8c)

Figure 8– Correlation between spread and shear threshold for Group 1, 2 and 3.

These results confirm those of several authors [8].

For the three cases of results shown in figure 8, it can be seen that there is indeed a correlation between the spreading results measured with the mini-cone and those measured with the rheometer. This representation, spread according to the shear threshold, for pasta formulated with the same ratio (W / (C + PM)) with the same quantity of water, without the viscosity agent, allows us to observe:

• the spread decreases with the increase of the shear threshold and thus the reduction
Of the SP.

• The spread decreases with the increase of the shear threshold and thus the decrease of the ratio (C / PM) is with the increase of the quantity of the marble powder.

4.2. Correlation between Spreading and Shear threshold of Group 4, 5 and 6 Results (with AV)

The results shown in figure 9 correspond to those of the correlations between the spreading results and the rheometer; results of pasta formulated with the same ratio (W / (C + PM)) is therefore with the same amount of water and a ratio C / PM = 2 in the presence of the viscosity agent.

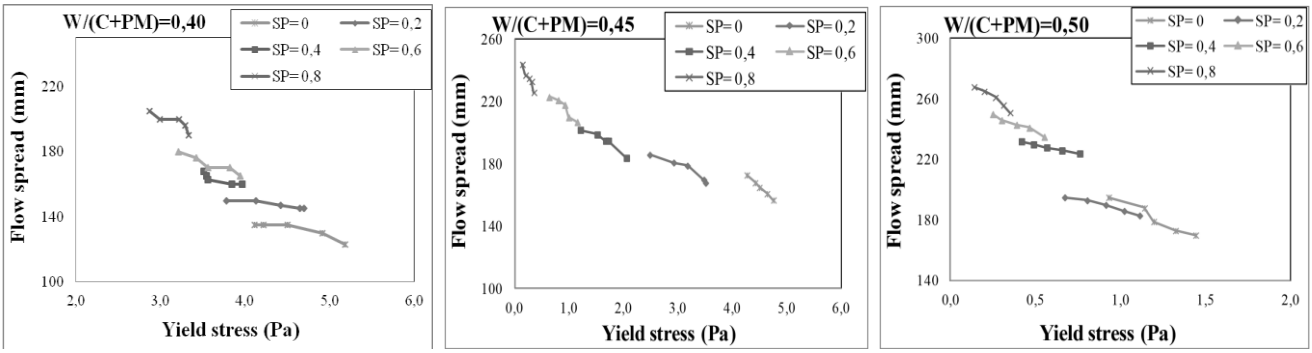

(9a) (9b) (9c)

Figure 9–Correlation between spread and shear threshold for Group 4,5 and 6

The results of figure 9 show that:

• The spread decreases with the increase of the shear threshold and therefore the increase of the VA.

• The spread decreases with the increase of the shear threshold and thus the reduction of the SP. In general, the measured shear threshold values do not exceed 10 Pa for all the pulps tested.

5. CONCLUSION

This study focused on the rheological behavior of self-placing cementitious pastes for which we have replaced a part of cement with marble powder from marble waste. Two test programs were conducted: the first using the mini-cone to measure pasta spreading; the second using the HAAKE RHEOSTRESS 1 rheometer to measure the shear threshold of the pasta.

According to the results obtained, it can be concluded that for the case of self-placing pastes, the higher the SP, the more the flow of these pastes approaches the Newtonian flow; it is due to the dispersing effect of (SP).

In terms of correlation, in general, spreading is a decreasing function of the shear threshold regardless of the value of the ratio W / (C + PM) and the C / PM ratio of the pasta. The increase in (SP) increases the spreading of pasta and lowers the shear threshold.

For pastes without (AV) and fixed (SP) a substitution of the cement by the marble powder decreases the spreading at the mini cone and increases the shear threshold.

The introduction of the viscosity agent into the different compositions does not have a great influence on the spreading measurements and the shear threshold measurements.

6. REFERENCES

[1]- Bury, Christensen. The role of innovative chemical admixtures in producing selfconsolidating concrete. Proceedings of the first North American conference on the design and use of self-consolidating concrete. 12-13 Novembre 2002. Chicago. pp 141-146.

[2]- Aïtcin P.C., Jiang S., Kim B.G. L'interaction ciment / superplastifiant Cas des polysulfonates. Bulletin des laboratoires des Ponts et Chaussées. Juillet-Août 2001. n° 233. pp 87-98.

[3]- De Larrard F. Structures granulaires et formulation des bétons. édition LCPC. 2000.

[4]- Roussel N. A theorical frame to study stability of fresh concrete. édition RILEM Material and structure 2006. Vol 39 (1). pp 75-83.

[5]- Ferraris C.F., Obla K.H and Hill R. The influence of mineral admixtures on the rheology of cement paste and concrete. Cement and concrete researchs. 2001. Vol 31. pp 245-255.

[6]- Messaoudi, F., Bouras, R., Sonebi, M., Kaci, S. "Investigation of Rheological Behaviour of Self- Compacting Marbled Paste", Proceedings of 6th North American Conference on the Design and Use of SCC Self-Consolidating Concrete (SCC) on the Design and Use of SCC Self-Consolidating Concrete and 8th RILEM International Symposium on Self-Compacting Concrete (SCC), USA, 2016, 9 p.

[7]- Phan T.H., chaouche M and Moranville M. Influence of organic admixtures on the rheological behaviour of cement pastes. Cement and Concrete Researchs. 2006. Vol 36. pp 1807-1813.

[8]- Bouras, Rachid, Chafiaa SI Hadj Mohand, and Mohammed Sonebi. "Adhesion and rheology of joints fresh mortars." Journal of Materials and Engineering Structures «JMES» 6.2 (2019): 157-165.

Revue des Matériaux et Energies Renouvelable Vol 5 N°2, 2021
ISSN : 2507-7554
***E*- ISSN** : 2661-7595

Revue des Matériaux
&
Energies Renouvelable

https://www.univ-relizane.dz
ISSN : 2507-7554
***E*- ISSN** : 2661-7595

FACULTE DES SCIENCES ET DE LA TECHNOLOGIE, UNIVERSITE DE RELIZANE.

NUMERICAL MODELING OF THE CRACK PROPAGATION FOR THE EVOLUTION OF THE STRAIN ENERGY ALLSE BY THE X-FEM METHOD

Open Access

Bentahar Mohammed*[1] *, Benzaama Habib*[2] *, Mahmoudi Noureddine*[3]*.

[1]*Laboratoire de biomécanique appliquée et de biomatériaux, ENPO Oran , Université Tahar Moulay de Saida, e-mail: bentahae@yahoo.fr : mohammed.bentahar@univ-saida.dz*
[2]*Laboratoire de biomécanique appliquée et de biomatériaux, ENPO, Ecole Nationale Polytechnique, Mechanical Engineering Department, Oran e-mail: habenza@yahoo.fr*
Université Tahar Moulay of Saida, Civil Engineering Department, e-mail: mahmoudi.noureddine@yahoo.fr / mahmoudi.noureddine@ univ-saida.dz

Article history:

Received 16 November 2020.

Received in revised form 17 November 2020.

Accepted 25 June 2021.

Keys word: 2D crack propagation, modelization, X-FEM, CPS4R, ALLSE

RESUME

In this article, the 2D extended finite element method (XFEM) in mode I, was used to model the crack propagation. this use based on modeling by the ABAQUS computer code. The quadratic elements with 4 CPS4R nodes were used to make this modelization. Two examples of meshs with different approximate overall sizes of the mesh one of 0.2 and the other of 0.5 were studied. In addition, the XFEM method was used to know the maximum value of the final crack load of the mesh. The evolution of the strain energy (ALLSE) was studied between the two cases.

1. Introduction

The extended finite element method, XFEM, is an evolution of the classical finite element method. This method was first developed by Belytschko and his colleagues in 1999 [1]. indeed, This method is based on the concept of unity partition. In fracture mechanics, the problems are treated by the classical finite element method, then by the XFEM introduced in Belytschko 1999, Moës 1999 [1,2]. on the other hand, J.L. Swedlow et al [3] used conventional finite elements to analyze the stress and elastoplastic deformation of a plate comprising a crack. On the other hand, Benzley [4]. Gifford and Hilton [5] developed the enriched finite elements, adding special analytical functions concerning the displacement of the nodes for the elements located in the area of the crack front. The advantage of these enriched finite elements is that the FIC can be directly calculated such as part of the results. Another method based on the classical FEM called the Extended Finite Element Method (XFEM), or the Generalized Finite Element Method, this method is an extension of the FEM, it has been applied to the problems of fracture mechanics since 1999. The crack propagation is simulated by replacing the elements newly crossed by a crack by a special element.

* *Corresponding author. bentahae@yahoo.fr*

Moës et al [2] present the 2D method which is based on the concept of unit partition (PUM), proposed by Melenk and Babuška [6], consists in enriching the approximation of the finite element method using of functions making it possible to better describe the field of displacement of a problem considered.
To model the dynamic rupture by numerical simulation, numerous publications have been carried out; (Duarte et al. [7]; Moës et al. [8]; Gravouil et al. [9], for the propagation of 2D cracks, (Dolbow et al. [10]) for contact problems, (Moës et al. Belytschko [11]) for cohesive areas, (Belytschko et al. [12] , Réthoré et al. [13], Song and Belytschko, [14]) for the use of different crack propagation criteria in the prediction of the growth path of crack by X-FEM.
Other works known in the literature which have developed the X-FEM method for the dynamic propagation of cracks, such as the work of Réthoré et al. [13,15,16,17], thus Grégoire et al. [19] Moës et al. [19] present the two-dimensional method. For quasi-static cases, this method was developed by Belytschko and Black [1]; Moës et al. [2]. The main idea of XFEM is to model the discontinuity the moving through the mesh, of the model with the help of enrichment of standard finite element shape functions. Dekker et al [20] presented a new approach based on the X-FEM method to deal with arbitrary crack paths. Rahman and Siegfried [21] studied the effects of particles as a reinforcement on the fatigue crack growth behavior of the Al 6061 / ZrO2 composite material by the (X-FEM) method. Others by, Guangwu et al [22] have used the X-FEM method to examine the effect of interphase thickness on the propagation of a predefined matrix crack. Bruce et al [23] summarized recent efforts to validate a cohesive zone X-FEM model with a mixed-mode PMMA fracture experiment.

2. X-FEM theory background

The extended finite element method (X-FEM) was initially introduced by Belytschko and Black (1999) [1]. They presented a method based on the finite element method for modeling of the crack propagation. This method does not need the re-engagement process.
In this process, discontinuous enriched functions are added to the approximation by finite elements for the crack demonstration and the crack develops arbitrarily in the finite element mesh. The most important and effective step towards improving the extended finite element method has been described by (Moëes et al., 1999) [2].
The existence of a crack in the extended finite element method, leads to two different enrichments in the interior problem of crack and enrichment of the crack tip.
The interior of the crack is enriched by a modified discontinuous Heaviside function (Eq. (2.1)), and the crack tip is enriched by using the functions presented in the equation (2.2) Belytschko and Black (1999) [1].

$$H(x) = \begin{cases} +1 & x > 0 \\ -1 & x < 0 \end{cases} \tag{2.1}$$

$$\{F_{i(r,\theta)}\}_{i=1,2,3,4} = \left\{\sqrt{r}\, sin\frac{\theta}{2}, \sqrt{r}\, cos\frac{\theta}{2}, \sqrt{r}\, sin\frac{\theta}{2}, \sqrt{r}\, cos\frac{\theta}{2} sin\theta\right\} \tag{2.2}$$

The function ($\sqrt{r}$ sin (θ/2)) is discontinuous, among these functions, which indicates the discontinuity of the function along two faces of the crack.
Where r and θ are the coordinates of x in the polar reference frame centred at the crack tip.

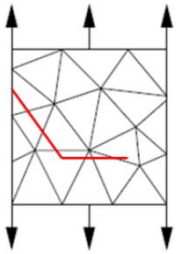

Figure 1- Schematic illustration of the numerical XFEM method for the analysis of a cracked body Duflot [24]

3. Elements modeling

In our model, the elements (CPE4R) with 4 bilinear nodes, reduced integration with hourglass control, was used to make the modeling of the evaluation of energy (ALLSE) of the propagation of the crack in 2D.

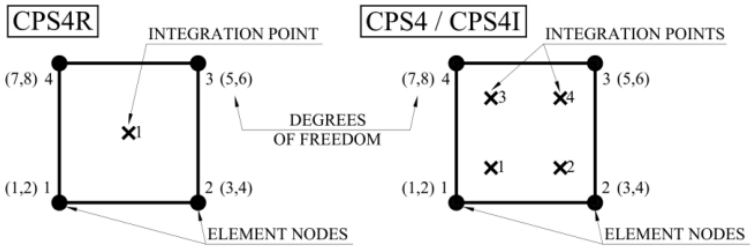

Figure 2- Plane stress elements of linear geometric order (first order) (author study based on Abaqus user manual)

The phenomenon is described more precisely in Cook et al [25] and in the Abaqus user manual.

4. Numerical model

The structure considered has a length L = 16 mm and a width C = 7 mm, with an initial crack (a = 1 mm). The parametric mesh and made up of 448 square elements of plane stress with four nodes of the type (CPS4R) and 495 nodes. The steel structure with E = $72x10^9$ Pa and ν = 0.3 is subjected to a tensile stress σ. A parametric mesh of approximately 0.2 and 0.5 overall size was used. The mesh admits an initial crack of dimension (a) being able to be modified according to the various values of the applied load. The mesh admits an initial crack of dimension (a) being able to be modified according to the various values of the applied load. The boundary conditions of the simulation of crack propagation are the following ones: the fixed support was applied to the lower surface of the structure (U1 = U2 = U3 = UR1 = UR2 = UR3 = 0), and the upper surface supports a stress load σ, the left border is blocked in the case of rotation. and the boundary condition is shown in Figure 3.

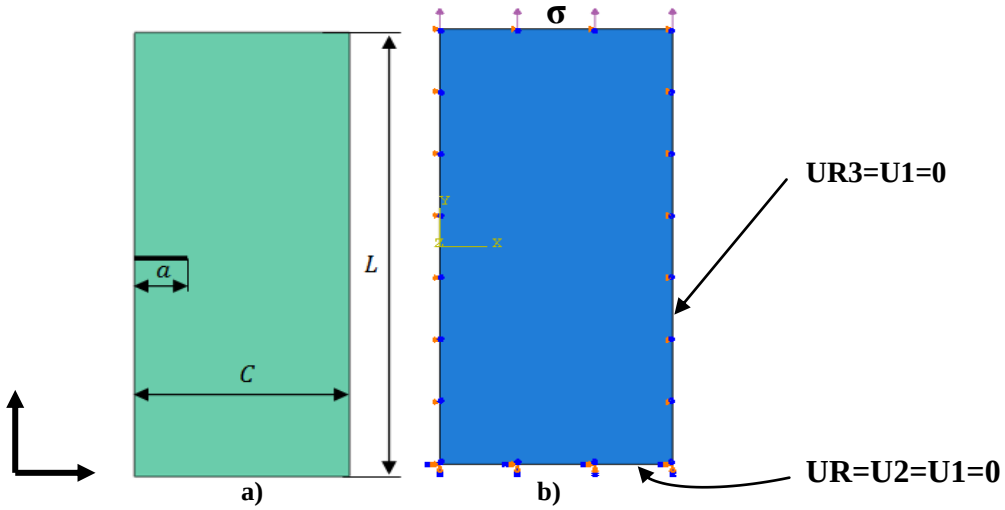

Figure 3- Model a) crack presentation b) Boundary conditions

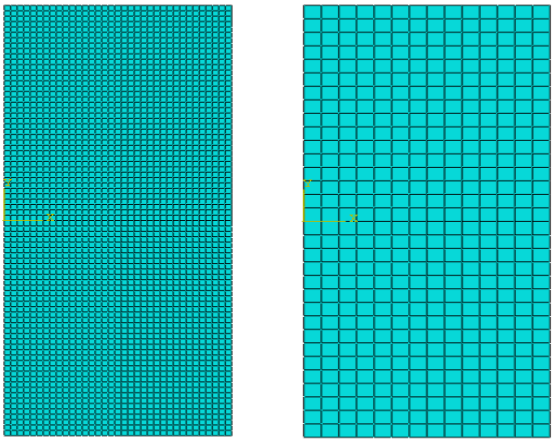

Figure 4- Model X-FEM a) mesh of approximate total size 0.2 b) mesh of approximate total size 0.5

4.1. Mesh for approximate overall size 0,5

The figure below presents the model XFEM concerning the unrefined mesh for an approximate value of 0.5 the study will be made in the various cases of crack propagation, having varying the values of the tensile stress σ which equals 50, 60 , 70, and 75Pa. Until the total crack of the Mesh.

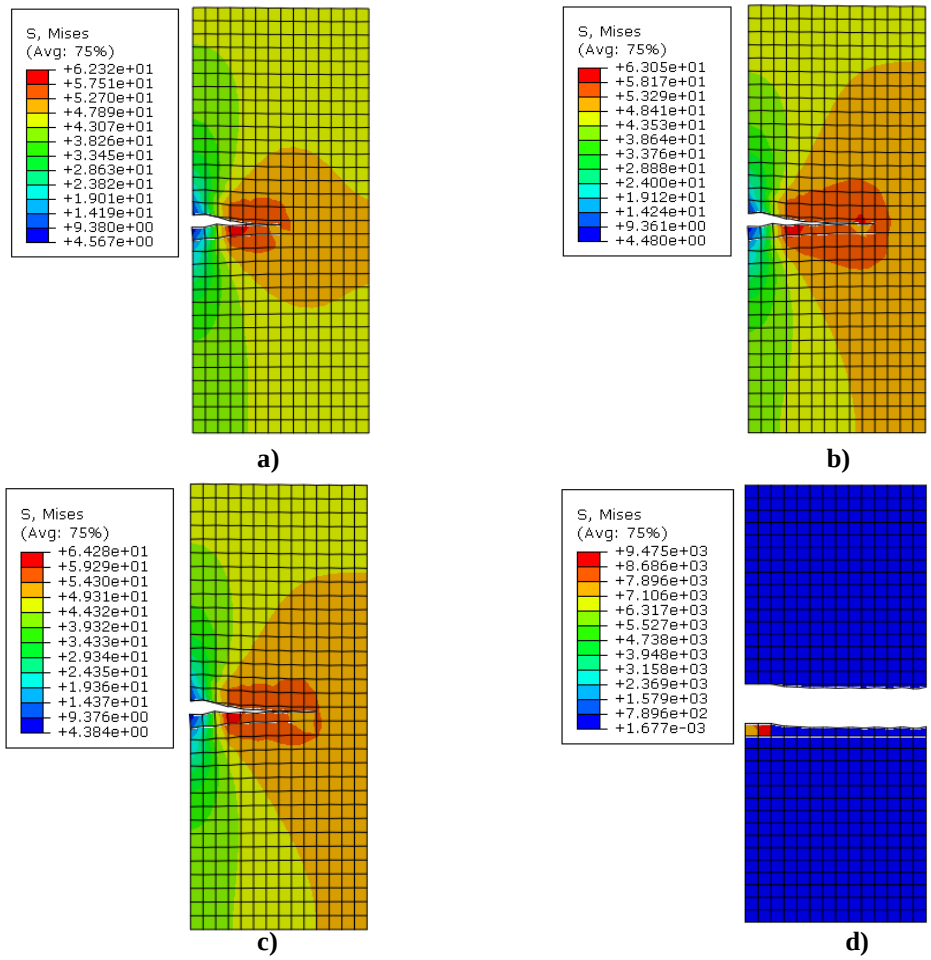

Figure 5- Model X-FEM for a Mesh of approximate total size 0.5 of mesh: a) 50N, b) 60N, c) 70N and d) 75N

4.2. Mesh for approximate overall size 0.2

The figure below presents the model XFEM concerning the mesh refined for an approximate value of 0.2. The study will be made in the various cases of crack propagation, one making varies the values of the tensile stress σ which equals 50, 60, 70, and 75Pa, and until the value of the total crack of the Mesh which equals 305Pa.

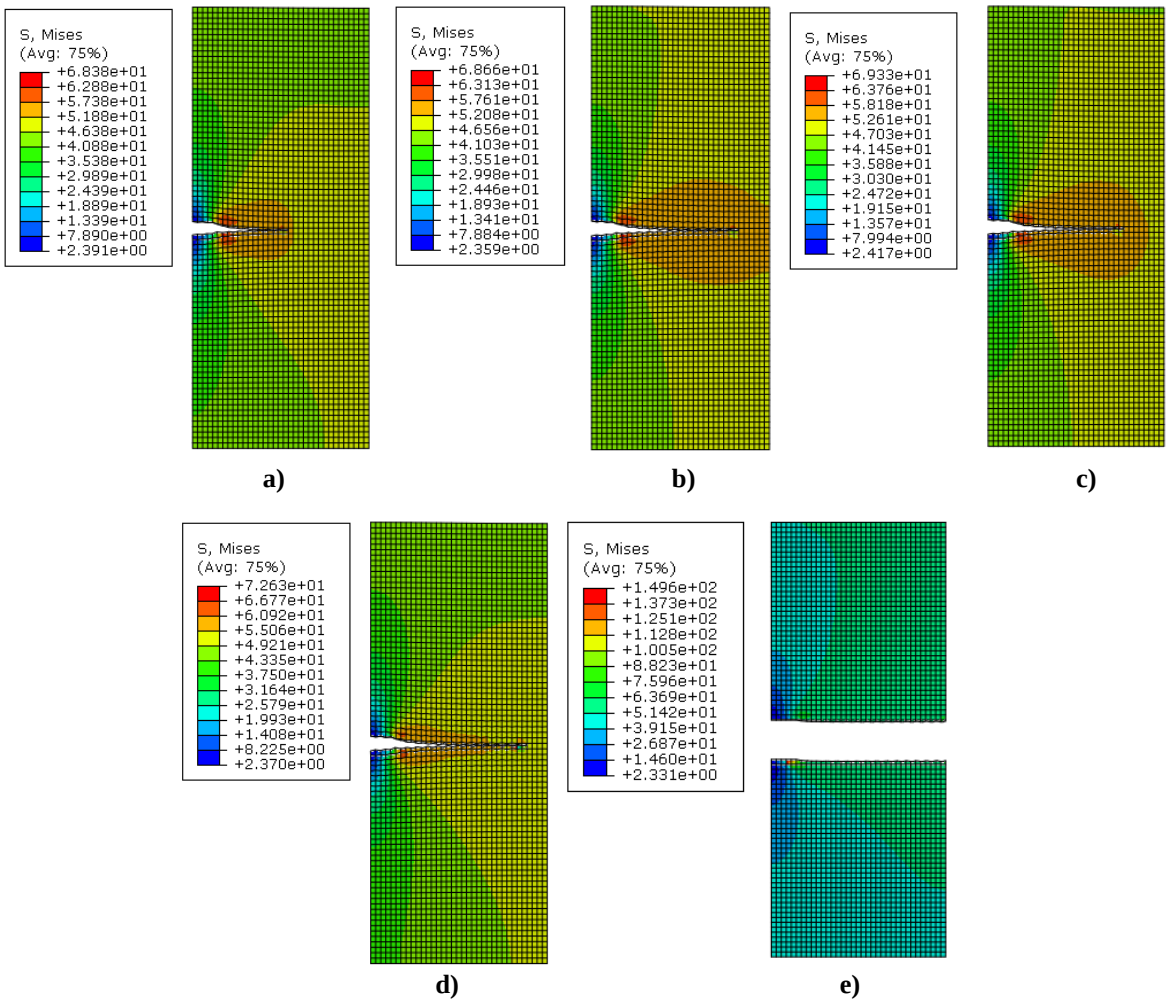

Figure 6- Model X-FEM for a mesh of approximate total size 0.2 of mesh a) 50N, b) 60N, c) 70N d) 75 and e) 305N

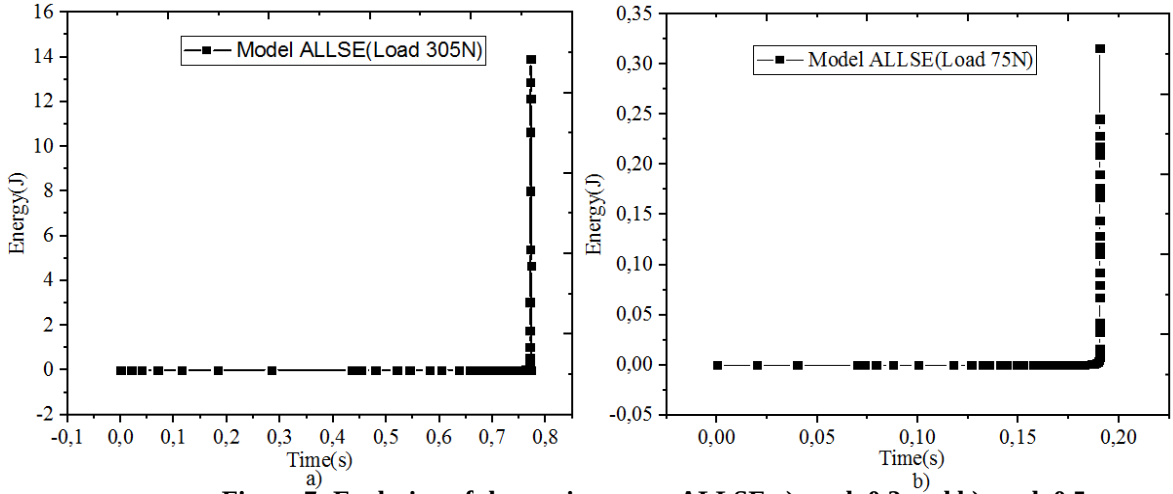

Figure 7- Evolution of the strain energy ALLSE a) mesh 0.2 and b) mesh 0.5

Figure 7 shows the evolution of the strain energy (ALLSE) as a function of time for the applied load of 305N (fig 7 (a)), and for the applied load of 75N (fig 7 (b)), we observe that the energy is linear horizontally and then vertically. However, there are similar results were obtained by Xiaodong et al [26].

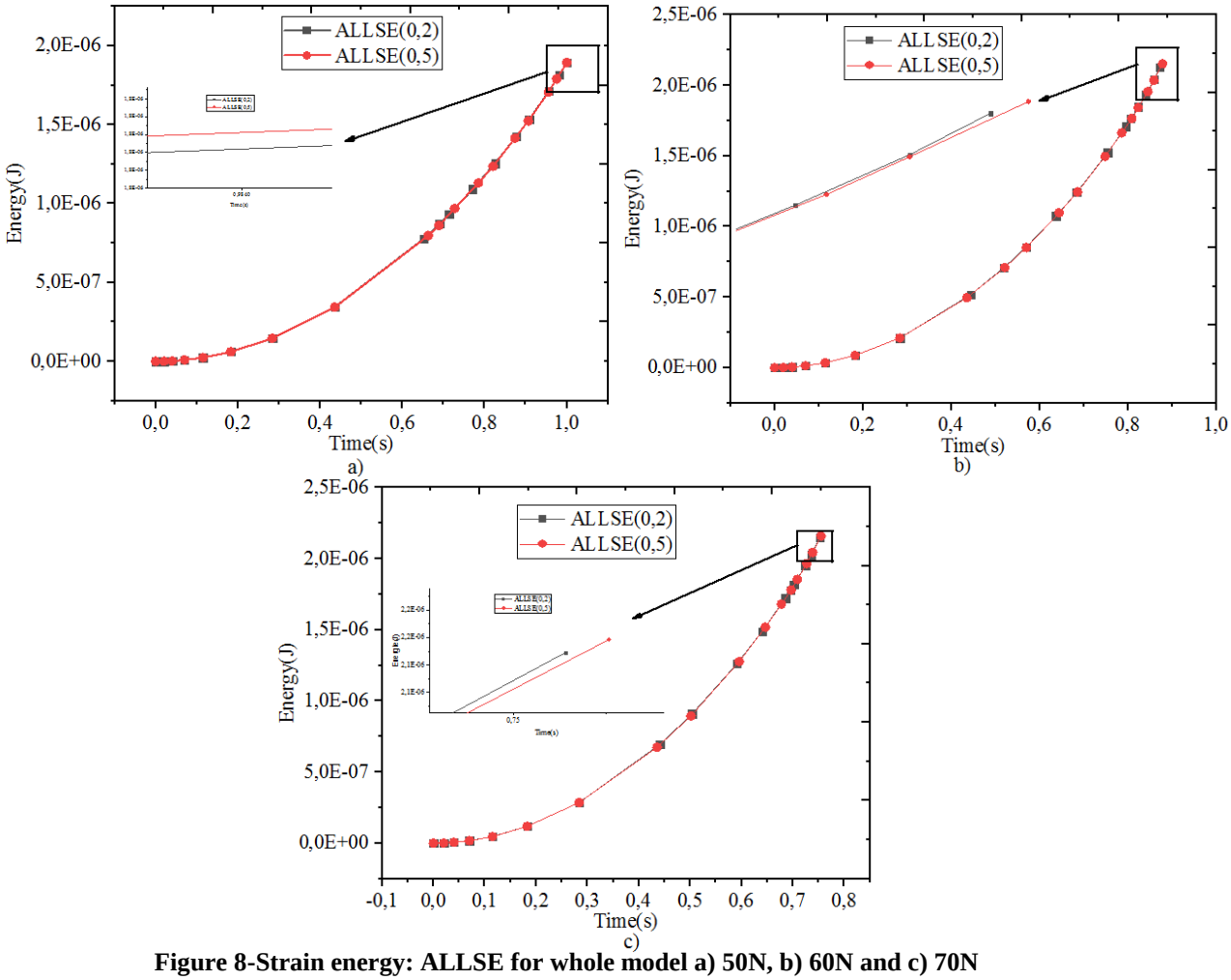

Figure 8-Strain energy: ALLSE for whole model a) 50N, b) 60N and c) 70N

Figure 8 presents the evolution of the strain energy (ALLSE) as a function of time for various approximate overall sizes of the mesh. Note that, a good match was obtained between the two comparison results. In addition, the increase in time causes an increase in energy for both cases.

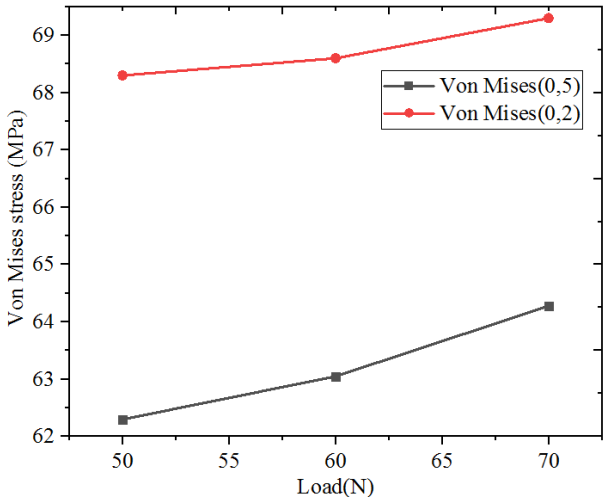

Figure 9- The comparison of the Von Mises stress between the two meshes

Figure 9 shows the evolution of the Von Mises stress for the two meshes one of approximate total size 0.2, and the other mesh of an approximate total size of 0.5. One obtains that the value of Von Mises of the mesh of an approximate overall size 0.2 is greater compared to the mesh of an approximate overalll size 0.5 (0.2> 0.5). Furthermore, the increase in the load causes an increase in the Vin Mises stress.

5. Conclusion

In this article, two meshes at different approximate overall sizes are compared using strain energy (ALLSE).
The extended finite element method X-FEM was used to model the evaluation of energy (ALLSE) of a problem of crack propagation in 2D.
The maximum value of the load for the total cracking of the mesh 0,2 is more superior, of that obtained in the case of a mesh of approximate total size 0,5.
Each load applied at a certain time increment.
a good correspondence was obtained between the two results of comparison concerning the evolution of the stress of Von Mises.

6. References

[1] T. Belytschko, T. Black, Elastic crack growth in finite element with minimal remeshing, International Journal for Numerical Methods in Engineering. 45 (1999) 601–620.
[2] N. Moës, J. Dolbow, T. Belytschko, A finite element method for crack growth without remeshing. International Journal for Numerical Methods in Engineering, 46(1999) 131–150.
[3] J.L. Swedlow, M.L. Williams, W.H. Yang, Elasto-plastic stresses and strains in cracked plate, Proc.1st.Int.Conf. Fracture, Sendai, Japan, 1(1965) 259-282.
[4] S. Benzly, Representation of singularities with isoperimetric finite elements. Int. J. Num. Meth. Engng, 8(1974) 537-545
[5] L.N. Gifford, P.D. Hilton, Stress intensity factors by enriched finite elements, Engineering Fracture Mechanics, 10 (1978) 485-496.
[6] I. BABUŠKA J. MELENK, The Partition of Unity Method. International Journal for Numerical Methods in Engineering, 40(1997) 727-758.
[7] C. Duarte, O. Hamzeh, T. Liszka, W. Tworzydlo, A generalized finite element method for the simulation of three-dimensional dynamic crack propagation. Computer Methods in Applied Mechanics and Engineering, 190(2001) 2227–2262
[8] N. Moës, A. Gravouil, T. Belytschko, Non-planar 3D crack growth by the extended finite element and level sets - Part I : Mechanical model. Int. J. Numer. Meth. Engng, 53(2002), 2549–2568.
[9] N. Moës, A. Gravouil, T. Belytschko, Non-planar 3D crack growth by the extended finite element and level sets - Part II : Level set update. International Journal for Numerical Methods in Engineering, 53(2002) 2569–2586.
[10] J. Dolbow, N. Moës, T. Belytschko, An extended finite element method for modeling crack growth with frictional contact. Computer Methods in Applied Mechanics and Engineering, 190, 51(2001.), 6825–6846.
[11] N. Moës, T. Belytschko,. Extended finite element method for cohesive crack growth. Engineering Fracture Mechanics, 69-7 (2002)813–833.
[12] T. Belytschko, H. Chen, J. Xu, G. Zi, Dynamic crack propagation based on loss of hyperbolicity and a new discontinuous enrichment, International Journal for Numerical Methods in Engineering, 58 (2003), pp. 1873-1905
[13] J. Réthoré, A. Gravouil, A. Combescure , An energy-conserving scheme for dynamic crack growth using extended finite element method , International Journal for Numerical Methods in Engineering, 63 (2005), pp. 631-659
[14] J.-H. Song, T. Belytschko, Cracking node method for dynamic fracture with finite elements, International Journal for Numerical Methods in Engineering, 77 (2009), pp. 360-385
[15] J. Réthoré, Méthodes élements finis étendus en espace et en temps : Application à la propagation dynamique des fissures. Ph.D. thesis, INSA-LYON(2005).
[16] J. Réthoré, A. Gravouil, A. Combescure, A stable numerical scheme for the finite element simulation of dynamic crack propagation with remeshing. Computer Methods in Applied Mechanics and Engineering, 193, 42-44 (2004) 4493–4510.
[17] J. Réthoré, A. Gravouil, A. Combescure, A combined space–time extended finite element method. International Journal for Numerical Methods in Engineering, 64(2005a) 260–284.
[18] D. Grégoire, H. Maigre, J. Réthoré, A. Combescure, Dynamic crack propagation under mixed-mode loading - Comparison between experiments and XFEM simulations. International Journal of Solids and Structures, 44 (20) (2007) 6517–6534.
[19] N. Moës, J. Dolbow, T. Belytschko, A finite element method for crack growth without remeshing. International Journal for Numerical Methods in Engineering, 46(1999) 131–150.
[20] R. Dekker, F.P. van der Meer, J. Maljaars, L.J. Sluys, A cohesive XFEM model for simulating fatigue crack growth under mixed-mode loading and overloading international journal for numerical methods in engineering, 118, 10(2019) 561-577.
[21] B. R. Rahman, S. Siegfried, XFEM SIMULATION OF FATIGUE CRACK GROWTH IN ALUMINUM ZIRCONIA REINFORCED COMPOSITES, International Journal for Multiscale Computational Engineering,17- 5(2019) 469-481
[22] F.Guangwu , G.Xiguang, S.Yingdong, XFEM analysis of crack propagation in fiber-reinforced ceramic matrix composites with different interphase thicknesses, Journal Composite Interfaces, 27- 3(2020) 327-340.
[23] G. Bruce, P-E. Matin, G. Robert, XFEM simulation of a mixed-mode fracture experiment in PMMA Engineering Fracture Mechanics, 229 -15(2020)106945.

[24] M. Duflot, Application of non-mesh methods in fracture mechanics. Doctoral thesis, University of Liège, 2004Y. Chuzel, INSA of Lyon, 2008.
[25] R. D. Cook, D. S. Malkus, M. E. Plesha, R. J. Witt, Concepts and Applications of FEA, 4 th ed,John Wiley&Sons, Inc(2002). (98–102).
[26] H.u. Xiaodong , J. Xu , **D.** Xiangmei ,Y. Zhang, F. Zhou **,** Research on Fatigue Crack Propagation of 304 Austenitic Stainless Steel Based on XFEM and CZM **Metals ,10-6** (2020) 727.

Revue des Matériaux et Energies Renouvelable Vol 5 N°2 , 2021.
ISSN : 2507-7554
***E*- ISSN** : 2661-7595

Revue des Matériaux & Energies Renouvelable
Journalhome : https://www.univ-relizane.dz
ISSN : 2507-7554
***E*- ISSN** : 2661-7595

FACULTE DES SCIENCES ET DE LA TECHNOLOGIE, UNIVERSITE DE RELIZANE.

Numerical Simulation of Forced Convection in Receiver of two Concentrators: dish parabolic and trough parabolic

Open Access

***Djermane Kenza*[1], *Kadri Syham*[1*]**

[1] *Laboratory of Semiconductor Devices Physics (LPDS), Department of Material Sciences, University of Bechar, P.O.B 417, 08000 Bechar,Algeria*

Article history:

Received 27 September 2020.

Received in revised form 28 September 2020.

Accepted 21 October 2020.

Keys word : *Dish parabolic ; Trough parabolic ; Receiver temperature ; Fluid ; Turbulent Forced convection ; Finite element method.*

RESUME

Solar concentrators use reflective mirrors parabolics or parabolic cylindrical to concentrate the solar rays respectively in a point or linear focus. In the point focus or along the linear focus are the receptors (absorbers) which capture the solar heat thus concentrated. The objective of our work is to study numerically the convective heat transfer in a receiver of a dish and trough parabolics in order to choose the best one for the cooling application of a photovoltaic module. The permanent forms of the Navier-Stokes equations, the continuity and energy equations are solved by the finite element method. The results obtained are presented in the form of average Nusselt number and receiver temperature will be presented for various combinations of Reynolds number. The results obtained show that the dish parabolic is better for our cooling application.

1. Introduction

Renewable energy is the only alternative to exhaustible natural resources, such as oil and gas…, it is also considered to be the main source in our life. The types of energy sources may vary according to their uses and applications in different fields. Solar concentrators are an important technology in the field of solar energy exploitation.There are two ways to harness energy from the sun. First is by using the concentrating solar thermal system. This is done by focusing the heat from the sun to produce steam. The steam will drove a generator to produce electricity. This type of configuration is normally employed in solar power plants. The other way of generating electricity is through a photovoltaic (PV) cell. This technology will convert the sunlight directly into electricity [2]. This technique is now being widely installed in the residential house and at remote places. It is also contributing to the significant increase in the development of Building Integrated Photovoltaic (BIPV) system. One of the parameters for determining which design is better will be based on how large an area can be captured and in respect to it the mass and complexity of its manufacturing. Scaling-up of first-generation technologies is one of the most important priorities as the basic principle of work is to focus sunlight from the much greater area into a

* *Corresponding author. E-mail address: syhammiss@yahoo.fr*

smaller area. Nevertheless, research in the field of solar concentration is far from over and presents a remarkable challenge for the future.

These systems can be seen in Figure 1. Solar towers and dishes use the principle of focusing sun rays at one point while troughs and Linear Fresnel Reflectors (LFR) focus sun rays into one line, which is usually designed as a pipe filled with molten salt. Different types of concentrators produce different peaks of temperatures and correspondingly varying thermodynamic efficiencies. This is due to differences in the way that they track the sun and focus light. New innovations in concentrated photovoltaic technology are creating those systems to become more and more cost-effective.

In concentrating collectors solar energy is optically concentrated before being transferred into heat. Concentration can be obtained by reflection or refraction of solar radiation by the use of mirrors or lens. The reflected or refracted light is concentrated in a focal zone, thus increasing the energy flux in the receiving target. Concentrating collectors can also be classified into non-imaging and imaging depending on whether the image of the sun is focused at the receiver or not. The concentrator belonging in the first category is the Compound Parabolic Collector(CPC); whereas all the other types of concentrators belong to the imaging type.The collectors falling in this category are:

1. Parabolic trough collector(PTC);
2. Linear Fresnel reflector(LFR);
3. Parabolic dish (PDR);
4. Central receiver.

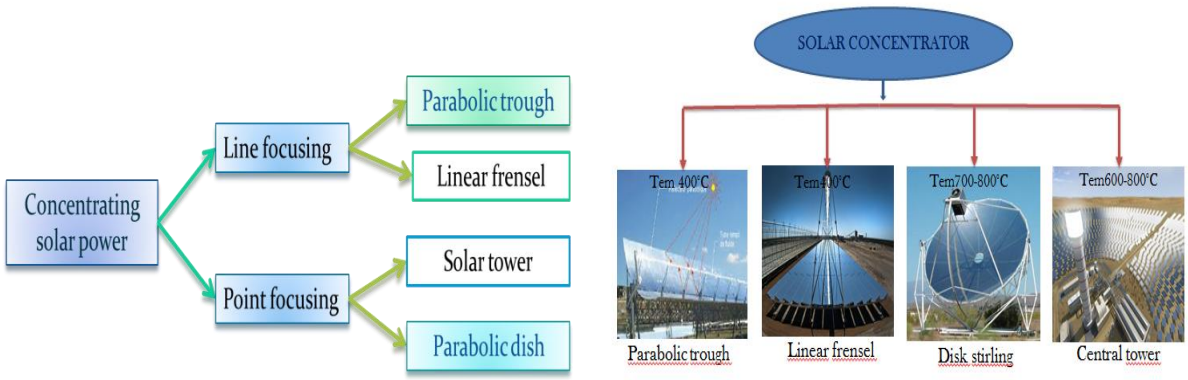

Figure 1– Types of CPV technology

The parabolic reflector is one of the most popular and important means of generating highly directional radiation[3]. At the macroscale, the broadband characteristics and simple design of parabolic reflectors have made them part of our daily lives, from automotive headlights and satellite dishes [4,5] to confocal microscopy and noptical single-molecule spectroscopy [6,7].

In this work we compared two types of concentrators in terms of forced convection and geometric optics. For this, this work is a test of two types of concentrators to safely place the solar module in the concentrator receiver. We seek to take the maximum solar radiation and avoid the degradation of the solar module placed by better cooling.

1.1. Parabolic dish

A parabolic dish reflector, shown schematically in Figure (2a), is a point-focus collector that tracks the sun in two axes, concentrating solar energy on to a receiver located at the focal point of the dish. The dish structure must track fully the sun to reflect the beam into the thermal receiver.For this purpose tracking mechanisms similar to the ones described in previous section are employed in double so as the collector is tracked in two axes[8].The receiver absorbs the radiant solar energy,

convertingit into thermal energy in a circulating fluid. The thermal energy can then either be converted into electricity using anengine-generator coupled directly to the receiver, or it can be transported through pipes to a central power-conversion system. Parabolic-dish systems can achieve temperatures inexcess of 1500°C. Because the receivers are distributed. Parabolic dishes have several important advantages, the most important of them : They are always pointing the sun, they are the most efficient of all collector systems,They have modular collector and receiver units that can either function independently or as part of a larger system of dishes.

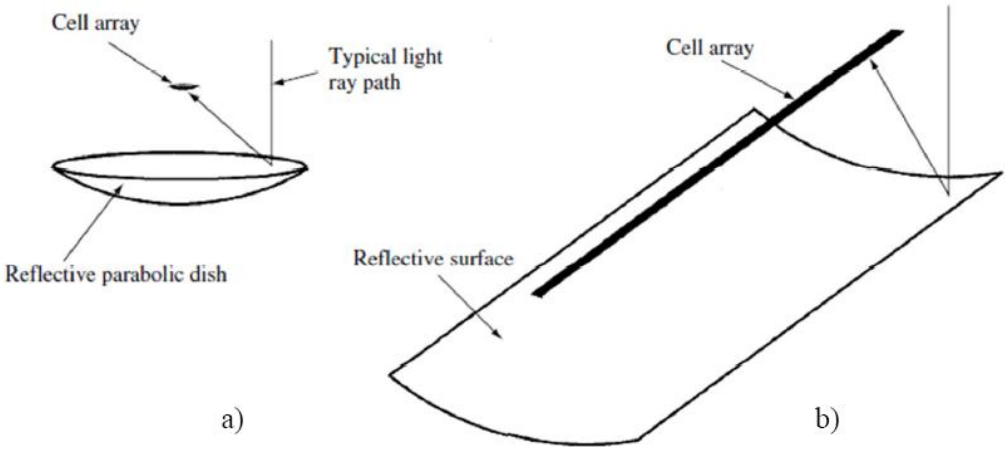

Figure 2– Reflective cocentrator configurations; a) parabolic dish, b) parabolic trough.

1.2. Parabolic trough

Concentrated photovoltaic system that uses a trough consists of a parabola troughed reflectors (mirrors), which concentrate sun rays into a focal point which is constructed as an absorber tube. The collector fields contain dozens of parallel rows of tubular collectors arranged along the axis (line) North-South. This configuration allows it to monitor the movement of the sun from east to west during days and provides constant focus on the sun (Figure 2b). Tracking of the sun is done by rotating reflectors around the absorber tube. Their position provides a constant reflection of the sun to absorber tube[8].The advantages of the former tracking mode is thatvery little collector adjustment is required during the dayand the full aperture always faces the sun at noon time butthe collector performance during the early and late hours ofthe day is greatly reduced due to large incidence angles (cosine loss). North–South orientated troughs have their highest cosine loss at noon and the lowest in the mornings and evenings when the sun is due east or due west.

2. Physical Model and Mathematical Formulation

2.1. Physical Model

Figure 3 illustrates the physical problem of the two concentrators chosen. It consists of rectangular cavities of different dimensions. For figure (3.a) represents the receiver of the parabolic trough which has the following dimensions: the length L_1 and the width H_1. The receiver of the parabolic dish is shown diagrammatically in figure (3.b) of length L_2 and width H_2. In both geometries there is water. The fluid is supposed Newtonian, incompressible and its thermophysical properties are constant. The fluid enters with uniform temperature, T_0 = 293 K, and velocity profiles at the inlet section and the tube length is appropriate in order to obtain fully developed profiles (of velocity and temperature) at the outlet section. The top horizontal wall is maintained at a heat flux equal to 50000 W/m^2 and the bottom horizontal wall is assumed to be adiabatic. Table 1 summarizes the boundary conditions of our problem.

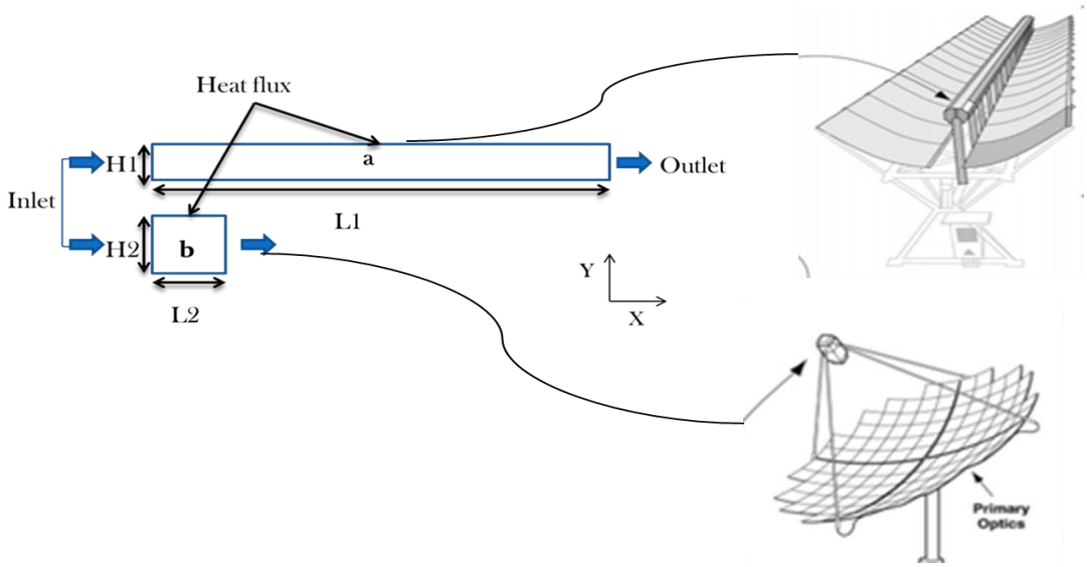

Figure 3– Physical model of the receiver : a)Parabolic trough collector ,b)Parabolic dish reflector

Table 1. Boundary conditions used in this simulation.

Walls	Boundaries conditions
The bottom horizontal wall	$U = V = \frac{\partial T}{\partial n} = 0$
The top horizontal wall	$q = 50000\ W/m^2$
Inlet	$\begin{cases} U = 1 \\ V = 0 \end{cases} \quad T = 0$
Outlet	$P = \frac{\partial T}{\partial n} = 0$

2.2. Mathematical Formulation

The coupled system of conservation equations describing the forced convection two-dimensional flow of the water is

$$\frac{\partial \mathrm{U}}{\partial \mathrm{x}} + \frac{\partial V}{\partial y} = 0 \tag{1}$$

$$U\frac{\partial U}{\partial x} + V\frac{\partial U}{\partial y} = -\frac{\partial P}{\partial x} + \frac{\mu_{hnf}}{\rho_{hnf}\nu_{nf}}\frac{1}{Re}\left(\frac{\partial^2 U}{\partial x^2} + \frac{\partial^2 U}{\partial y^2}\right) \tag{2}$$

$$U\frac{\partial V}{\partial x} + V\frac{\partial V}{\partial y} = -\frac{\partial P}{\partial x} + \frac{\mu_{hnf}}{\rho_{hnf}}\frac{1}{Re}\left(\frac{\partial^2 V}{\partial x^2} + \frac{\partial^2 V}{\partial y^2}\right) \tag{3}$$

$$U\frac{\partial T}{\partial x} + V\frac{\partial T}{\partial y} = \frac{K_{hnf}}{K_f}\frac{1}{Pr.Re}\left(\frac{\partial^2 T}{\partial x^2} + \frac{\partial^2 T}{\partial y^2}\right) \tag{4}$$

wirtten in dimensionless forms as:

For the flow is turbulent, we chose the k-ε model proposed by Launder and Spalding [8]. This model introduces the turbulent kinetic energy (Eq. (5)) and the rate of dissipation (Eq. (6)). These equations can be expressed in the following form:

$$\nabla . \left(\rho_m \vec{V}_m k\right) = \nabla . \left(\frac{\mu_{t,m}}{\sigma_k} \nabla k\right) + G_{k,m} - \rho_m \varepsilon \quad (5)$$

$$\nabla . \left(\rho_m \vec{V}_m \varepsilon\right) = \nabla . \left(\frac{\mu_{t,m}}{\sigma_k} \nabla \varepsilon\right) + \frac{\varepsilon}{\kappa}(C_1 G_{k,m} - C_2 \rho_m \varepsilon) \quad (6)$$

Where$\mu_{t,m}$ is the eddy viscosity that is defined as:

$$\mu_{t,m} = \rho_m C_\mu \frac{k^2}{\varepsilon} \quad (7)$$

$$G_{k,m} = \mu_{t,m} \left(\nabla \vec{V}_m + \left(\nabla \vec{V}_m\right)^T\right) \quad (8)$$

With $C_1 = 1.44,\ C_2 = 1.92,\ C_\mu = 0.09,\ \sigma_k = 1,\ \sigma_\varepsilon = 1.3.$

$G_{k,m}$is the generation of turbulent kinetic energy due to the mean velocity gradients. In our simulation, both turbulent kinetic energy and dissipation of turbulent kinetic energy are equal to zero.

To solve the system of differential equations (1)–(4), with appropriate boundary conditions, the Galerkin finite element method is used. The two-dimensional spatial domain is divided into triangular elements (unstructured mesh) and a Lagrange-quadratic interpolation has been chosen.

To study the optimal reflector system with pure water, the following parameters are fixed: Prandlt number Pr=7, Reynolds number varies between 10000≤*Re*≤20000. The thermophysical properties of the water are represented in table 2.

Table 2. Water thermal properties at T = 300°K of [10]

Physical properties	**Water**
C_p(J.Kg^{-1}.K^{-1})	**4179**
ρ (Kg.m^{-3})	**997.1**
K(W.m^{-1}.K^{-1})	**0.613**
β×10^{-5} (K^{-1})	**21**

Based on the dimensions of the photovoltaic module chosen, we offer the characteristics of the parabolic dish and troughare represented in Table 3.

Table 3. Characteristics of the parabolic dish and trough

Parameter	Parabolic dish	Parabolic trough
Collector rim angle	45[deg]	45[deg]
Collector aperture	0.5 [m]	1[m]
length of a receiver (L)	0.2 [m]	1[m]
width of a receiver (H)	0.15 [m]	0.01 [m]
a design wavelength (λ_0)	600 [nm]	600 [nm]

Figure 4 shows the variation of the concentration ratio in the focal plane for the parabolic dish (a) and the parabolic trough (b). We notice that the concentration ratio for the parabolic dish is much higher compared to the trough parabolic. We can be explained by the different between point focusing and line focusing, this is what we need to put the solar module to can take the maximum of solar radiation.

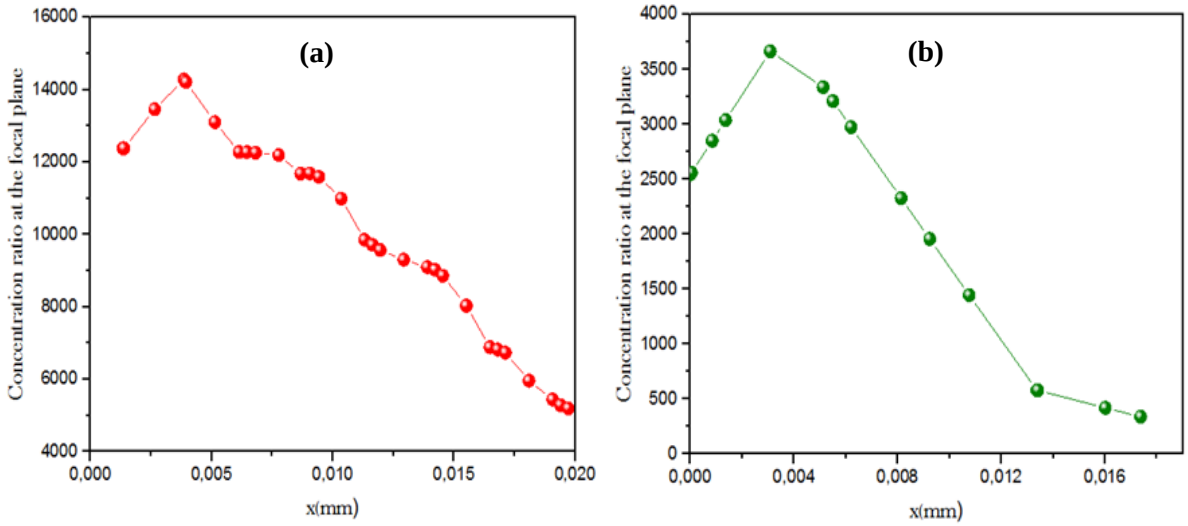

Figure 4– Concentration ratio at the focal plane of: a) the parabolic dish ,b) the parabolic trough

Figure 5 illustrates the effect of the Reynolds number on the average Nusselt number for the two types of concentrators. As Re increases, the average Nusselt number improves. For the parabolic dish, the average Nusselt number reaches a value of 200 for Re = 20000, on the other hand the parabolic trough does not exceed 140. The difference between the types is 30%, which shows that the convection is better in the parabolic dish. It is therefore noted that this type is more suitable for the cooling application of CPV systems. In addition, we can conclude that, if the receiver length is smaller, the cooling is better.

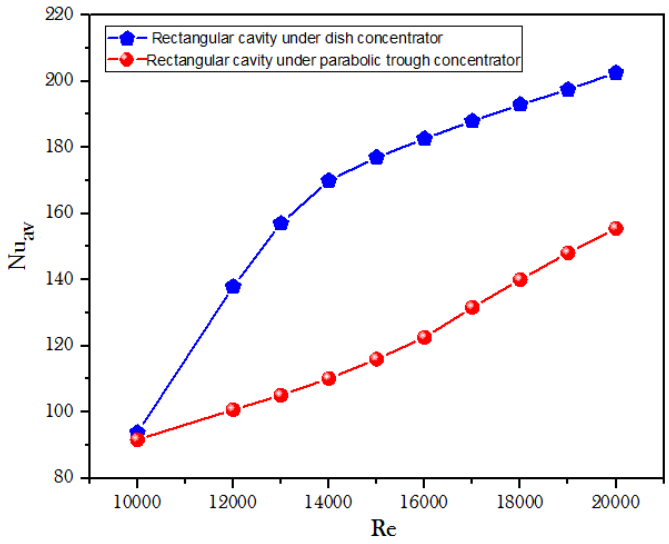

Figure 5– Comparison between the average Nusselt number of the parabolic dish (red online) and of the parabolic trough (green online)

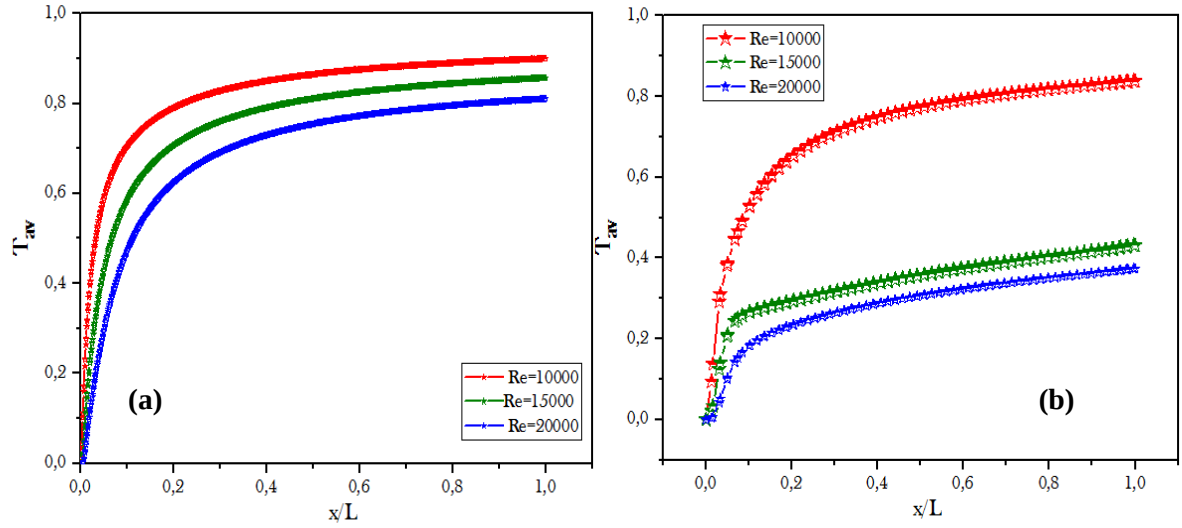

Figure 6– The receiver temperature versus Reynolds numbers of: a) the parabolic trough, b) the parabolic dish

The evolution of the fluid temperature along the receiver at different Reynolds number values for the parabolic trough (a) and the parabolic dish (b) is shown in figure 6. For the two types of concentrators, the temperature of the receiver decreases with the increase in Reynolds number. In addition, it can be observed that the receiver temperature of the parabolic trough is greater than the temperature of receiver of the parabolic dish. This confirms the previous remarks. We find that for the dish parabolic and increasing the Reynolds number, the temperature of the receiver decreases in a significant way. This ensures the choice of the parabolic dish for the good cooling of the concentrated photovoltaic module.

3. Conclusion

In this article, we have presented the numerical simulation of forced convection in a receiver of a solar concentrator: parabolic dish and parabolic trough. Our main objective of this work is to choose the best concentrator for our cooling application of a photovoltaic module, which is placed in the place of the receiver. The major problem is the high temperature, which requires a cooling system. When the convective heat transfer is favored, we confirm the good cooling of our module.

The results obtained show that the parabolic dish concentrates solar radiation rather than the parabolic trough. In addition, the variation of average Nusselt number and temperature confirms that the parabolic dish favors the convective mode and consequently a good cooling of our module. We can conclude that the optimal concentrator in our application is the dish parabolic.

4. REFERENCES

[1]- N.J. Ekins-Daukes, 2009, Solar Energy for Heat and Electricity: The Potential for Mitigating Climate Change, No 1: 1-12.

[2]- Harry penketh, 2019, Optimal position of an emitter in a wavelength-scale parabolic reflector, Vol. 58, No. 29, AppliedOptics.

[3]- M. A. Lieb and A. J. Meixner, 2001, A high numerical aperture parabolic mirror as imaging device for confocal microscopy, 8,458–474, Opt. Express.

[4]- J. Stadler, C. Stanciu, C. Stupperich, and A. J. Meixner, 2008, Tighter focusing with a parabolic mirror, 33, 681–683, Opt. Lett.

[5]- A. Kalogirou, 2004, Solar thermal collectors and applications Soteris, 30, 231–295, Progress in Energy and Combustion Science.

[6]- B. Ghasemi, S.M. Aminossadati, 2010, Periodic natural convection in a nanofluid-filled enclosure with oscillating heat flux, Vol. 49, pp. 1–9, International Journal of Thermal Sciences.

[7]- B. E. Launder and D. B. Spalding, 1974, The numerical computation of turbulent flows, Vol. 3, No. 2, pp. 269–289, Computer Methods in Applied Mechanics and Engineering.

[8]- Charly GAY, François LANZETTA, Daniel HISSEL, Michel FEIDT, 2012, Représentation Énergétique Macroscopique (REM) d'un moteur Stirling en vue d'une hybridation thermique.

[9]- C.H Lin and W.L Hsieh, 2012, Optimization of PhotovoltaicPenetration in Distribution Systems Considering Annual Duration Curve of Solar Irradiation, Power Systems, Vol.27, Issue: 2, IEEE Transactions.